Excitation-induced structural instability of semiconductor surfaces

2006 J. Phys.: Condens. Matter 18 S1479

(http://iopscience.iop.org/0953-8984/18/30/S07)

INSTITUTE OF PHYSICS PUBLISHING JOURNAL OF PHYSICS: CONDENSED MATTER

J. Phys.: Condens. Matter **18** (2006) S1479–S1516 doi:10.1088/0953-8984/18/30/S07

Excitation-induced structural instability of semiconductor surfaces

Katsumi Tanimura and Jun'ichi Kanasaki

The Institute of Scientific and Industrial Research, Osaka University, Mihogaoka 8-1, Ibaraki, Osaka 567-0047, Japan

Received 30 December 2005, in final form 30 May 2006
Published 14 July 2006
Online at stacks.iop.org/JPhysCM/18/S1479

Abstract

The present work reviews laser-induced electronic processes of structural instability on covalent semiconductor surfaces. In particular, we concentrate on the mechanism of the instability that takes place at the intrinsic sites of reconstructed surface structures. In order to elucidate the primary processes involved, we focus our attention on experimental results obtained by scanning tunnelling spectroscopy studies, to reveal surface structural changes at the atomic level, and by post-ionization spectroscopy studies, to probe desorption processes with high sensitivity. First, the results obtained for reconstructed Si surfaces and {110} surfaces of III–V compound semiconductors are systematically surveyed. The instability is characterized by local bond rupture at intrinsic surface sites that show important common features. Also, we find significantly different aspects of the instability, which depend on the basic properties of surfaces. Based on the characteristics revealed by the experimental results, we then propose a mechanistic model based on the generalized two-hole localization mechanism, and demonstrate, through the quantitative analysis of typical experimental results, that the model describes all the important features quantitatively and consistently.

(Some figures in this article are in colour only in the electronic version)

1. Introduction

The surfaces of covalent semiconductors undergo drastic reconstructions, governed by the balance between the energy gained from variations in the bonding properties and the elastic-energy loss due to distortions from ideal sp^3 bonding [1]. Reconstructed surfaces show structural and electronic properties significantly different from those in bulk crystals, and exhibit several surface-specific phenomena such as structural instability under electronic excitation. As demonstrated by several recent studies, laser excitation induces electronic bond rupture, which leads to drastic changes in semiconductor surface structure and desorption of constituent atoms [2–12]. This structural instability induced by electronic excitation,

excitation-induced structural instability, is intrinsic in the sense that atoms at perfect surface sites are subject to bond rupture [3–8, 10–12]. Therefore, studies to elucidate the fundamental mechanism of the instability are important not only for the basic research of light–matter interaction, but also for deeper understanding of the physical properties of semiconductor surfaces. Furthermore, it is a key issue for non-thermal engineering of surfaces to fabricate functionalized surfaces [13]. In fact, the interaction of laser light with solid surfaces has been studied extensively, motivated by applications in materials processing [14].

Previously, laser-induced effects on silicon surfaces attracted particular interest, partly for understanding the mechanism of laser annealing phenomena in this material. Becker *et al* first studied laser-induced structural changes on the Si(111)-(7 × 7) surface using scanning tunnelling microscopy (STM), and found a new class of *c*-(4 × 2) and (2 × 2) structures [15]. The laser fluence Φ used was about 1 J cm^{-2}, which is certainly above the melt threshold. Consequently, the structural transformation was attributed to laser-induced melting followed by rapid re-crystallization. Stritzker *et al* measured time-of-flight (TOF) spectra of Si atoms emitted from Si surfaces under the irradiation of laser pulses with Φ of 1–2 J cm^{-2} [16], and showed that the translational energy of desorbed Si atoms increased with fluence. The observed fluence-dependent translational energy of desorbed Si atoms has been regarded as a consequence of surface melting. Thus, the major structural changes on Si surfaces induced by laser irradiation were ascribed to laser-induced melting for fluences exceeding a threshold value [17].

On the other hand, laser-stimulated desorption (LSD) below the melt threshold was studied for several MX compound semiconductors. In these studies, it was shown that the monatomic and diatomic nonmetallic species are emitted as major products, together with monatomic metallic species [18, 19]. The yields of these neutral species often show a highly super-linear dependence on the laser intensity. Several models of the electronic mechanisms were proposed based on these results [18–20]. However, for establishing a basic understanding of the electronic mechanism of LSD, the following aspects needed clarification: (1) the initial bonding properties of atoms to be desorbed, (2) the electronic transition that triggers the desorption, and (3) the origin of the instability that causes bond breaking and desorption, as often pointed out in studies of desorption induced by electronic transitions [21]. In view of these criteria, earlier studies of LSD, by means of quadrupole-mass spectrometers (QMSs), usually had serious drawbacks related to the poor sensitivity of this method of detection. To observe desorbates with a reasonable signal-to-noise ratio with QMS, one must remove typically a few monolayers (ML) per laser pulse. Therefore, desorption always takes place from highly damaged surfaces. For such cases, it is difficult not only to identify the initial bonding configurations of atoms to be desorbed, but also to specify electronic transitions responsible for the desorption processes. Consequently, the poor sensitivity of QMS gave us less than ideal situations to analyse the results to reveal primary processes responsible for the bond breaking and desorption. A second drawback concerns the gas-phase dynamics after desorption. As analysed theoretically, the densities of laser-induced desorbed particles per unit volume per unit time in vacuum were high enough to induce collisions among emitted species, leading to Knudsen-layer formation [22]. By this process after desorption, several important characteristics of the desorption process were lost or modified significantly.

Later, highly sensitive detection methods of post-ionization techniques were introduced in order to solve these drawbacks. Resonance ionization spectroscopy (RIS), in which neutral species emitted are ionized by nanosecond laser pulses via resonance-enhanced multiphoton absorption processes [6, 7, 20, 23], has been applied mainly for metallic neutral species desorbed from compound semiconductor surfaces and Si atoms from Si surfaces. Although the studies by means of RIS have revealed some interesting aspects of LSD, it is not

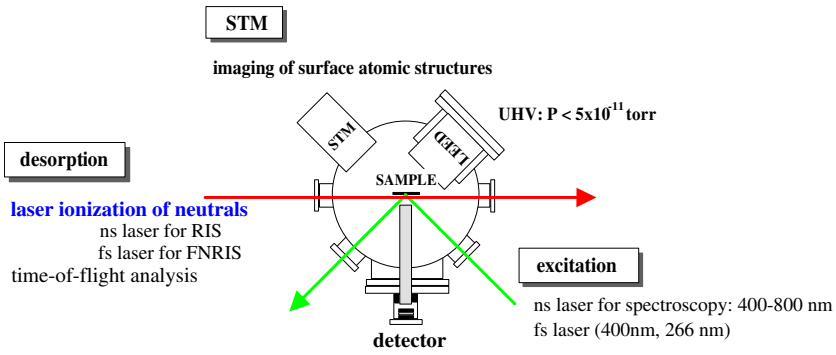

Figure 1. Schematic representation of experimental set-up used in the series of studies on the excitation-induced structural instability on covalent semiconductor surfaces. Specimens, prepared in an ultra-high vacuum (UHV) chamber with a base pressure of 5×10^{-11} Torr, were excited by laser pulses, and desorbed neutral species were detected with high sensitivity by means of RIS or FNRIS. Surface structures prior to and after laser excitation were probed *in situ* by direct atomic imaging with a UHV-STM to elucidate laser-induced changes at the atomic level.

enough to obtain full information on the desorption process from compound semiconductor surfaces, since the important knowledge of the nonmetallic species, which have high ionization energies, has been completely absent in most cases, or has been obtained only in the higher-fluence regime [24]. Then, as a new detection method, femtosecond non-resonant ionization spectroscopy (FNRIS) was introduced to detect all neutral species emitted upon surface excitation simultaneously and with high sensitivity [10, 12, 25].

These sophisticated experimental techniques to detect neutral desorbates have a sensitivity of typically 10^{-7} monolayer (ML) per pulse, thus making it possible to study desorption processes without changing original surface structures. However, such desorption studies should be combined with the studies to characterize surface structures, at the atomic level, in order to reveal precisely the initial bonding configurations of atoms to be desorbed. Based on the fundamental knowledge, together with spectroscopic studies to identify the optical transition that triggers the desorption, one can understand the mechanism of the instability that causes bond breaking, desorption, and surface structural changes.

In this paper, we review our results obtained in a series of studies for laser-induced electronic processes on semiconductor surfaces along this line of strategy. After describing briefly the experimental methods employed in section 2, we describe main results systematically for Si(111)-(7 × 7), Si(001)-(2 × 1), Si(111)-(2 × 1), and InP(110)-(1 × 1) in sections 3 and 4. After clarifying the common and different features of the results on these semiconductor surfaces, we then propose in section 5 a theoretical model of the excitation-induced instability based on the two-hole localization mechanism. We will demonstrate that the proposed model describes systematically and consistently the available experimental results through quantitative analysis of typical experimental results.

2. Experimental details

In figure 1, we show a schematic diagram of experimental methods used in the series of studies. Specimens, prepared in an ultra-high vacuum (UHV) chamber with a base pressure of 5×10^{-11} Torr, were excited by laser pulses, and desorbed neutral species were detected with high sensitivity by means of RIS or FNRIS. Surface structures prior to and after laser

excitation were probed *in situ* by direct atomic imaging with a UHV-STM to elucidate laser-induced changes at the atomic level.

Prior to laser excitation, the atomic structures of the prepared surfaces were characterized mostly by STM measurements, and LEED and AES techniques were also used in some cases. Laser pulses generated by several laser systems were guided to the UHV chamber on the same optical path determined by using several apertures, and were incident at 45° from the normal of the surfaces. The laser beams were focused to ∼0.1 mm diameter on the surfaces by a quartz lens, and the intensity of each pulse was monitored by a calibrated photodiode. The fluence on the surface was evaluated by the energy per pulse and irradiation radius at which the beam intensity decreases from the peak intensity to $1/e$. Lasers used for generating ns laser pulses were an excimer-laser pumped dye laser (20 ns pulse width), a Q-switched Nd:YAG laser pumped dye laser (5 ns pulse width), and an optical parametric generator pumped by a Q-switched Nd:YAG laser (3 ns pulse width). Femtosecond laser pulses with a temporal width of 80–200 fs were generated with a Ti:sapphire laser equipped with a regenerative amplifier.

Neutral species desorbed from the surfaces upon excitation were detected using RIS and FNRIS. In RIS, neutral Si atoms desorbed from Si surfaces were resonantly two-photon ionized by ns laser pulses, which were guided to pass parallel to the sample surface. Si^+ ions thus ionized were collected by a negatively biased drift tube, and then detected by a microchannel plate placed in a shield box behind the drift tube. In FNRIS, the neutral atoms ejected from surfaces were ionized non-resonantly by intense fs laser pulses of 800 nm with a temporal width of 80 fs. The laser pulses for ionizing desorbed neutral species were guided to pass parallel to the sample surface. Ions ionized by laser pulses were collected and detected, similar to the case of RIS measurements. For both highly sensitive detection methods, time-of-flight (TOF) spectra of desorbed species were measured by changing the time delay of the pulses for ionization with respect to the incidence of laser pulses for surface excitation by using a delay generator. The system sensitivity of 10^{-7} ML per excitation-laser pulse was estimated for both RIS and FNRIS [25].

We used several specimens, which have the following characteristics. Boron-doped p-type Si(111) and Si(001) wafers with a resistivity ρ of 20 Ω cm and with a thickness of 0.5 mm were used for studying Si(111)-(7 × 7) and for Si(001)-(2 × 1). Standard cleaning procedures were applied for these surfaces. To prepare Si(111)-(2 × 1), a 0.2 mm thick P-doped n-type Si wafer with ρ of 3.15 Ω cm and B-doped p-type Si wafer with ρ of 1.3 Ω cm were cleaved in a UHV chamber. For InP(110)-(1 × 1) and GaAs(110)-(1 × 1), 0.2 mm thick wafers were used. The doping concentrations were 5.8×10^{18} cm^{-3} Zn for p-type InP, 8×10^{17} cm^{-3} Zn for p-type GaAs, 7.5×10^{18} cm^{-3} S for n-type InP, and 5×10^{18} cm^{-3} Si for n-type GaAs. They were cleaved in a UHV chamber, similar to the case of Si(111)-(2 × 1).

3. Excitation-induced structural instability on Si(111)-(7 × 7)

3.1. STM observation of laser-irradiated Si(111)-(7 × 7)

The Si(111)-(7 × 7) surface is a typical example of a reconstructed semiconductor surface, to which extensive studies have been carried out both experimentally and theoretically [1]. According to the dimer–adatom–stacking fault (DAS) model [26], this reconstructed surface consists of a unit cell of 12 adatoms, 42 first-layer atoms and nine dimers. This large-scale relaxation, together with associated charge transfer among dangling bonds, results in the formation of several surface-specific electronic states [1, 27]. The dangling bonds of adatoms form the S_1/U_1 state, which is located in the bulk bandgap. The back-bonds of adatoms form an occupied surface band (S_3) and an un-occupied U_2 band. The filled lone pair bonds of rest atoms form the dispersion-less S_2 band 0.8 eV below the Fermi level.

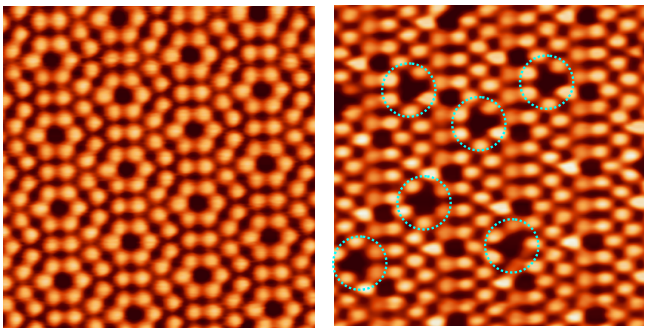

(a) (b)

Figure 2. STM images of the Si(111)-(7 × 7) surfaces (a) prior to and (b) after irradiation of 600 nm laser pulses at a constant fluence of 23 mJ cm^{-2}. The images were acquired at −2.0 V sample-bias voltage. White circles indicate the adatom sites where vacancies are formed.

For this surface, laser-induced electronic bond rupture of adatoms has been demonstrated by combining direct imaging of atomic structures by STM with highly sensitive detection of desorbed Si atoms [3, 6, 7, 28]. As a typical example of STM images displaying structural changes, we show in figure 2 the images acquired before, (a), and after, (b), laser-pulse excitation at 600 nm and a fluence of 23 mJ cm^{-2} (1.1 MW cm^{-2} in intensity). It is evident that the fluence is far below the typical melt threshold of 1 J cm^{-2}. As clearly seen in figure 2(a), the surface prior to excitation includes few surface vacancies (typically less than 10^{-3} ML). On the other hand, several dark spots are formed at adatom sites after irradiation. These dark spots are observed at the same positions irrespective of polarity of applied bias voltage between the tip and surface. Therefore, they can be assigned to missing adatom sites (adatom vacancies), rather than adsorbates that can display dark spots only in one polarity. This identification is confirmed by quantitative comparison of the STM results with the results of highly sensitive detection of Si-atom desorption, as described later.

One of the important characteristics seen in figure 2 is that laser-induced adatom vacancies are formed mostly at individual adatom sites, leaving the (7 × 7) structure essentially unchanged. It is estimated from a formula provided in [29] that 20 ns laser irradiation with the fluence of 200 mJ cm^{-2} at all wavelengths from 400 to 700 nm increases the temperature at the surfaces to about 640 °C, which is well below the melting temperature. In fact, all of the STM images obtained show no trace of surface melting and no indication of new reconstructions characteristic of melted surfaces [15]. Therefore, one can conclude that the laser-induced formation of adatom vacancies is not due to laser-induced surface melting, but to an electronic mechanism. Thus, figure 2 shows conclusively that electronic bond rupture occurs at intrinsic surface sites of a reconstructed semiconductor surface.

In order to have deeper insight into the laser-induced electronic process on Si(111)-(7×7), STM images were acquired systematically for surfaces irradiated with dye-laser pulses at wavelengths from 400 to 700 nm, and statistical analysis was undertaken by surveying over more than 1200 unit cells in the irradiated region [3, 6]. The analysis has revealed the following three important features of this electronic process.

The first feature is the site-dependent efficiency of adatom-bond rupture. The adatom sites of a unit cell of (7 × 7) structure are not equivalent, and they can be classified into four different sites: centre- or corner-adatom site on the faulted or unfaulted half. Substantial differences in the electronic properties have been demonstrated for adatoms on faulted and unfaulted halves [30]. In order to examine possible effects of this difference on bond-rupture efficiency, we studied the statistics on adatom–vacancy sites for the two halves. However, no significant differences were observed. On the other hand, when we compared the efficiency at centre-adatom sites with that at corner-adatom sites, we found a remarkable difference:

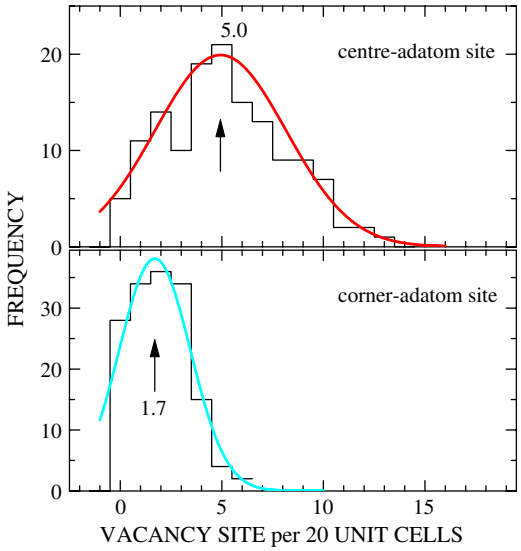

Figure 3. The histogram of the number of vacancies per 20 unit cells at (a) centre- and (b) corner-adatom sites, respectively, on the surface irradiated with 500 nm laser pulses at a constant fluence of 90 mJ cm^{-2} (after [3]).

centre-adatom sites show an enhanced efficiency of vacancy formation over corner-adatom sites. In figure 3, we show the histogram of the concentration of laser-induced adatom vacancies per 20 unit cells at (a) centre- and (b) corner-adatom sites [3]. It is evident in the figure that the mean value of the vacancy concentration at the centre-adatom site is three times larger than that at the corner-adatom site, far beyond the statistic error of sampling.

We show in figure 4(a) the concentration V of laser-induced adatom vacancies (in units of the fraction relative to the total number of adatom sites in the region surveyed) as a function of the number m of 600 nm laser pulses ($\Phi = 23$ mJ cm^{-2}) incident on the surface under repeated irradiation [6]. V increases linearly with m up to a level where 6% of the total adatoms have been removed. In figure 4(b) is shown the ratio of V at the corner-adatom sites to that at centre-adatom sites on the irradiated surface; it shows a constant value of 0.3 irrespective of m. Therefore, the site-sensitive efficiency of adatom–vacancy formation is not due to any accumulated effects under repeated irradiation, but is a direct consequence of the process that takes place within each laser pulse. The site-dependent efficiency with a ratio of about 0.3 was the case for irradiation at various fluences and at different wavelengths. Therefore, this is characteristic of the final step of the bond breaking process, independent of excitation wavelength and intensity.

The result shown in figures 3 and 4 has demonstrated clearly that the centre adatom is more reactive than the corner adatoms in the electronic bond rupture induced by laser excitation. According to the DAS model of the (7×7) structure, centre and corner adatoms are associated with two different geometric environments. The centre-adatom site has two rest atoms as neighbours, while the corner-adatom site has only one. Also, a centre adatom is adjacent to only one dimer, while a corner adatom is adjacent two dimers. Consequently, the dangling bond of the corner adatom has a higher density of occupied states than that of the centre adatom [30]. The difference in the electron occupation, ascribed to the different amount of charge transfer to the rest-atom dangling bonds, may give substantial changes in bonding properties. In fact, Uchida *et al* have found that centre adatoms are more frequently removed than corner adatoms in their atom-extraction experiments by STM tips [31]. Therefore, the site-sensitive efficiency of bond rupture can be taken as a consequence of the different bonding properties of the two adatom sites.

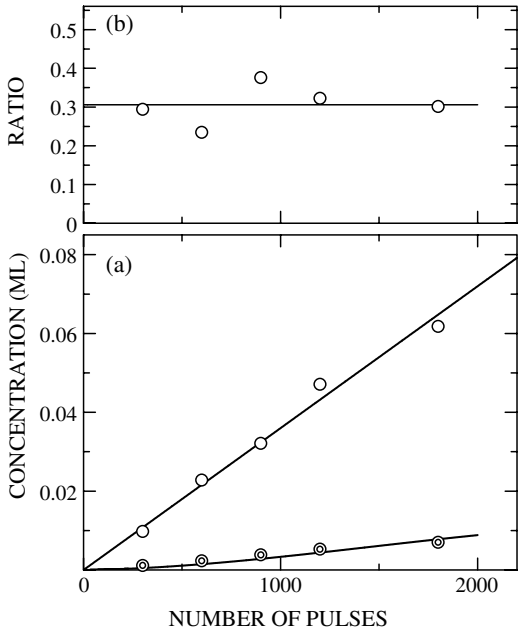

Figure 4. (a) The concentration of laser-induced adatom vacancies (open circles), and that of the dimer vacancies (double circles) as a function of the number of 600 nm laser pulses at a fluence 23 mJ cm^{-2} under repeated irradiation. For the growth of dimer vacancies, a result of Monte Carlo simulation (solid curve) is also shown under random formation of adatom vacancies. (b) The ratio of the number of vacancies formed at the corner-adatom site relative to that at the centre-adatom site as a function of the number of 600 nm laser pulses (after [6]).

The second feature of the electronic bond rupture on Si(111)-(7 × 7) is that the rate of bond rupture depends super-linearly on the excitation intensity. In figure 4(a), it is clear that V increases linearly with increasing m. In the figure, we also plotted the concentrations of dimer vacancies, which are adatom vacancies formed at nearest neighbour surface sites. The yield of the dimer vacancies coincides with that predicted from the statistics of random formation of vacancies, as shown by the solid curve in the figure. Therefore, the electronic bond rupture on this surface is characterized by the process that takes place at individual adatom sites without any site correlations. This feature manifests itself in the linear relation between V and m in figure 4(a). Based on the linear relation, we can define unambiguously the rate K of adatom–vacancy formation per single shot of a laser pulse with a given Φ. In the case of $\Phi = 23$ mJ cm^{-2}, it is 5×10^{-5} ML/pulse. In figure 5, the evaluated Ks are plotted as a function of Φ for 600 nm excitation. The rate shows a super-linear dependence on Φ (or the excitation intensity I_{ex}), thus revealing a second unique feature of laser-induced electronic bond rupture on semiconductor surfaces. We discuss extensively, in the last section, the origin of the super-linear dependence of K on I_{ex}, and argue that the dependence originates from non-linear interaction of photogenerated excited species. The solid curve in figure 5 is the calculated result of the theoretical model proposed in section 5.

Here we mention briefly, for completeness, the third important feature of the wavelength-dependent rate of bond rupture. Our statistical analysis of STM observations of surfaces irradiated at different wavelengths shows qualitatively the same features as those at 600 nm; the concentration V of laser-induced adatom vacancies increases in proportion to the number m of laser pulses, and the rate K of adatom–vacancy formation per single shot of a laser pulse

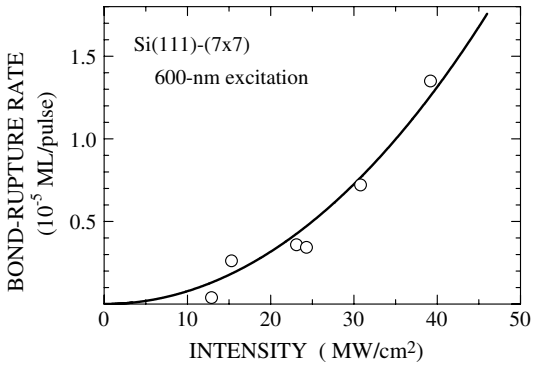

Figure 5. Excitation-intensity dependence of the rate of adatom–vacancy formation per pulse for the excitation of Si(111)-(7 × 7) at 600 nm. The solid curve is the results of theoretical calculation by using the proposed model (see the text).

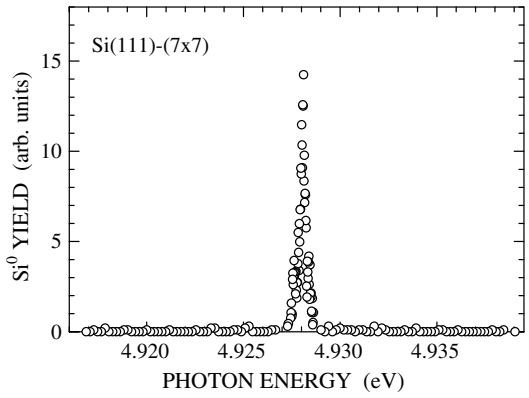

Figure 6. The ion yield as a function of photon energy of the ionization-laser pulses. The surfaces were excited with 200 fs laser pulses at 406 nm (after [32]).

shows super-linear dependence on the excitation intensity. However, the absolute value of the rate depends strongly on the excitation wavelength; the rate at 500 nm is less than one-tenth of that at 600 nm for a given fluence. We describe this feature, in detail, in the next section, since the desorption results show it more clearly.

3.2. Si-atom desorption upon laser excitation of Si(111)-(7 × 7)

3.2.1. General features. As shown in section 3.1, the amount of Si-atom removal per incident laser pulse is typically 10^{-5} ML. Therefore, highly sensitive detection of desorbed species is essential in order to obtain comprehensive information on the electronic bond-rupture of adatoms on Si(111)-(7 × 7). The RIS technique was extensively used to study the desorption induced not only by ns-pulse excitation [6], but also fs-pulse excitation [7, 32]. The detection system in RIS was sensitive enough to detect a small number of ions ($<10^{-7}$ ML) if they were emitted directly from the surfaces. However, when the ionization laser was absent, no ion signals were detected following surface excitation with either ns or fs laser pulses, leading to the conclusion that no ionic species were desorbed at the intensity range used in the studies. On the other hand, when the ionization laser was present, signals due to neutral species were clearly detected. Figure 6 shows the intensities of detected ion signals as a function of the photon energy of the ionization laser following surface excitation. It is clear in the figure that the RIS signal shows a resonance enhancement at 4.928 eV, which corresponds to the $^3P_0$–$^3P_1$ transition of ground state Si atoms [32]. Therefore, the species desorbed by surface excitation is the ground state Si atoms.

The kinetic energy distribution of desorbed Si atoms was studied by measuring TOF spectra for surface excitation with ns and fs laser pulses at different intensities and at different wavelengths. Although desorption yields change, depending on several characteristics of excitation laser pulses, the shape of the TOF spectrum with a peak flight time of 2.1 μs does not depend on wavelength, fluence, or temporal laser-pulse width [7]. Since the number of Si atoms desorbed by a single pulse is at most 10^{-4} ML, any effects of gas-phase collisions after desorption can be neglected [22]. Therefore, the energy distribution is characteristic of the bond breaking process at the surface. This fluence-independent kinetic energy, of desorbed Si atoms, contrasts strongly with laser-induced surface melting results [16], and proves the electronic nature of the Si-atom desorption from Si(111)-(7 $\times$ 7). Also, this feature indicates clearly that the final step of the bond rupture, which governs the energy partition to Si atoms, is common for any type of excitation.

The yield Y of Si-atom desorption, measured at the peak flight time as a function of m or of Φ, has been compared with the bond rupture rate K determined by STM studies. Under repeated irradiation at a constant Φ, Y was constant irrespective of m [28]. This constant Y corresponds to a constant K, which leads to a linear growth of adatom–vacancy concentrations. On the other hand, Y shows the same super-linear dependence on Φ as K; it increases almost quadratically in the low fluence regime, but exponentially in the high fluence regime [6, 28]. These results have proven that desorption of ground-state Si atoms is a direct consequence of the bond rupture of adatoms on the (7 $\times$ 7) surface. Thus, the initial bonding configuration has been clearly identified in the laser-induced electronic desorption of Si adatoms from Si(111)-(7 $\times$ 7).

3.2.2. Wavelength dependence of desorption efficiency. As mentioned in the introduction, identification of the electronic transition that triggers the desorption is crucial to understand the mechanism of a desorption process. Based on the definite correlation between the desorption yield Y and the bond-rupture rate per pulse K described above, the excitation-wavelength dependence of Si-atom desorption was studied extensively to identify the electronic transition [6]. The yield of Si-atom desorption, measured as a function of fluence for wavelengths ranging from 400 to 700 nm, showed similar super-linear dependence on the fluence Φ. However, the yield at a given fluence was strongly dependent on excitation wavelength. In order to quantify the wavelength dependence, a practical definition of the 'desorption efficiency' has been introduced, which is the desorption yield at a fixed fluence, since the usual definition of efficiency cannot be used because of the super-linear behaviour. The desorption efficiency thus determined is plotted as a function of the photon energy in figure 7. A strong enhancement is evident at 2.0 eV, with a weak and broad contribution above 2.5 eV. There is no 2.0 eV peak in the optical spectra of Si crystals [33]. Therefore, the peak structure is not related to any linear bulk-optical transition. An alternative assignment may be argued, that the 2 eV peak is related to two-photon absorption, based on the 4.185 eV direct bandgap energy at the Γ point [34], and that Y depends on Φ nearly quadratically at least in the weak fluence regime [6]. However, the Si-desorption yield under 4.66 eV laser excitation, which is above the direct bandgap, shows a similar super-linear dependence on Φ [7], thus excluding this alternative.

On the other hand, one can find two possible optical transitions involving surface-specific electronic states of the Si(111)-(7 $\times$ 7) surface [35–39], both of which show peak energies around 2.0 eV. One is the transition from the surface band S_2 to U_2, and the other is that from S_3 to U_1. The coincidence between the surface transition energies and the peak energy of the desorption enhancement suggests strongly an important role of surface electronic transitions on the adatom-bond rupture. Here we simply emphasize that the efficiency of desorption of

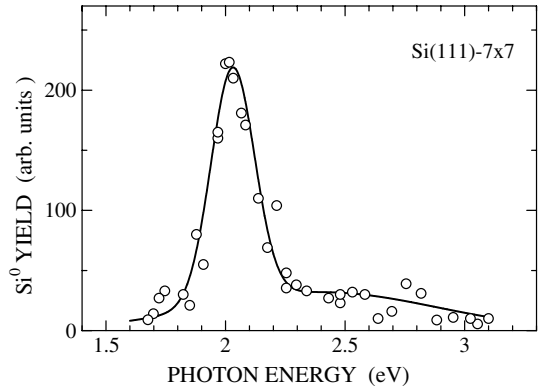

Figure 7. Photon-energy dependence of the desorption efficiency of Si atoms from the Si(111)-(7 × 7) surface (after [6]).

Si atoms on Si(111)-(7 × 7) depends resonantly on excitation wavelength, leaving extensive discussion of this feature to the last section.

The quantitative comparison of yields of Si-atom desorption for ns and fs laser excitations at the same wavelengths has given us some hints at the physics underlying the super-linear dependence of the rate. Such comparisons have been made at 403 and 266 nm [7, 32]. Although Y depends super-linearly on the excitation intensity I_{ex} for both ns and fs laser pulses, the magnitude of the yield is enhanced strongly for fs-pulse excitation when scaled in terms of fluence Φ. One can expect that the 100 fs temporal widths of fs laser pulses are shorter than the decay times τ of excited species responsible for the bond rupture. Therefore, in the case of fs-pulse excitation, the maximum density n_f is given by $n_f = \alpha\Phi$, where α is the absorption coefficient at a given wavelength. On the other hand, for ns laser excitation with temporal width w, which is longer than τ, the maximum density n_n can be estimated to be $n_n = \alpha\Phi(\tau/w)$, resulting in a significantly reduced excited-state density per unit time. Therefore, the density of the excited states and super-linear dependence of the rate of bond rupture is closely related. The role of excitation density in the bond-rupture rate will be discussed extensively in section 5.

3.2.3. Bond-breaking process: a phonon-kick model. Even without going into details of the mechanism of the instability, we can have some deeper insight into the final step of the bond rupture by analysing the Si-atom kinetic energy distribution. As described in section 3.2.1, the shape of TOF spectra of desorbed Si atoms is not dependent on wavelength, fluence, or temporal width of the excitation laser pulse. This feature implies that the same localized excited state leading to desorption (we refer to the state as the reactive state) is formed at adatom sites with formation yields depending on several characteristics of excitation-laser light.

The kinetic energy corresponding to the time at the peak of TOF spectra is 0.15 eV, which is much smaller than photon energies of excitation laser light. This low kinetic energy of desorbed Si atoms may exclude any desorption models which assume simple repulsive potential energy surfaces leading to the energy of around 1 eV. Also, the fluence-independent velocity distribution of desorbed Si atoms indicates clearly that the mechanism of desorption induced by multiple electronic transition (DIMET), often argued for desorption processes on metal surfaces [40, 41], is not the case for the adatom-bond rupture.

As demonstrated by STM results, the bond rupture on Si(111)-(7 × 7) takes place at individual adatom sites. Therefore, it is essential that some excited species localize to form the reactive state at individual adatom sites. In semiconductors, it has been well documented that defect reactions are induced (or enhanced) upon carrier localization at defect sites by generating transiently violent lattice vibration (phonon kick) [42]. Experiments [43] and *ab*

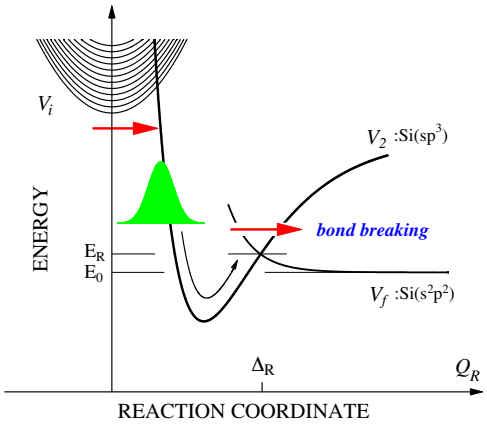

Figure 8. Schematic diagram of the model of the phonon-kick process for adatom-bond rupture on Si(111)-(7 × 7). Adiabatic potentials V_i, V_2, and V_f represent an excited state consisting of many delocalized excited species, the reactive state, and the final state of the bond breaking including a Si atom in the electronic ground state in vacuum, respectively. The reaction coordinate Q_R corresponds to the vibrational motion of adatoms normal to the surface (after [7]).

initio calculations [43–45] have shown a significant charge delocalization of dangling bond states of the adatoms, which results in a bonding interaction between adatoms and the Si atoms directly below them. The localization of excited species induces charge re-distributions around adatoms, and the bonding property may be affected seriously to weaken the bond, which can lead to a strong adatom vibration. Based on this consideration, the phonon-kick mechanism has been proposed for the bond breaking of adatoms [7]. In this model, upon formation of the reactive state, the violent vibration is induced along the reaction coordinate Q_R of vibrational motion of adatoms normal to the surface. This process is schematically portrayed in figure 8. In the figure, a group of parabolas denoted by V_i represents an excited state consisting of many delocalized excited species, V_2 represents the reactive state formed upon carrier localization, and V_f represents the final state. The electronic transition from V_2 to V_f governs the desorption probability, since the adatom electronic state of a perturbed sp^3-like configuration is finally transformed into the free-atom s^{2}p^2 state in V_f in the desorption. In the figure, it has been assumed that the transition takes place at a critical point R with an energy E_R and a distortion Δ_R on Q_R.

In terms of the potential energy diagram in figure 8, the phonon-kick process can be described as follows: the packet formed on the coordinate with a mean total energy $E_i(\geqslant E_R)$ passes the critical point j times with the energy $E(\leqslant E_i)$ during relaxation, induces the transition with a probability $P(E)$ at each passage, and finally dissipates. The Si atom desorbed by the packet with E has translational energy e given by $e = E - E_0$, where E_0 is the energy of V_f measured from the bottom of V_2. The number density $N(e)$ is determined by the product of j and $P(E)$, both of which are dependent on E. When a simple damping oscillator is assumed as the packet, j is inversely proportional to E. $P(E)$ can be evaluated by Landau–Zener formula [46]

$$P_{\mathrm{LZ}} = \{1 - \exp(-2\pi T^2/\hbar v_R\,|F_R|\}, \tag{1}$$

where T is the transition matrix element, $|F_R|$ is the change of the energy separation of the surfaces at R, and v_R is the velocity of the packet at R, respectively. P_{LZ} takes the largest value for $v_R = 0$ (i.e., $E = E_R$), with a sharp cut-off for $E < E_R$. For $E > E_R$, P_{LZ} decreases with increasing E.

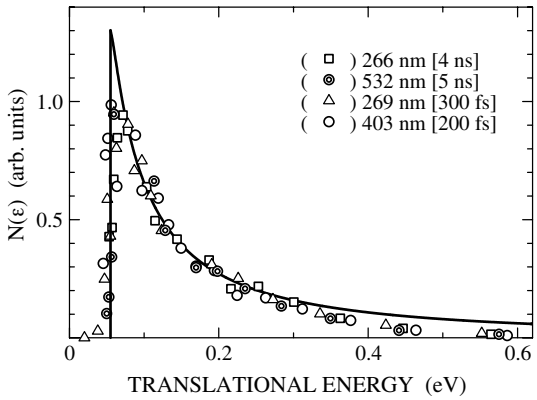

Figure 9. Translational energy distribution of Si atoms desorbed by the laser-induced electronic bond rupture of adatoms on Si(111)-(7 × 7). Surface excitation was performed at 300 K with laser pulses of different wavelengths, fluences, and temporal widths. Data for different types of laser light are normalized to the same peak height. The solid curve is the calculated distribution by the simple model presented in the text (after [7]).

In order to compare the consequences of this one-dimensional model with the experimental TOF results, we evaluated the number density $N(e)$ of atoms with translational energy e from the TOF spectrum, taking a phase space factor of v^2 into account (v is the speed) [47, 48]. The result is shown in figure 9.[1] The distribution shows a steep increase after an onset energy of about 0.02 eV to form a peak at 0.06 eV, associated with a decreasing high-energy tail up to 0.6 eV, thus displaying all the qualitative features predicted by the phonon-kick model. In view of the model in figure 8, the peak energy of 0.06 eV in $N(e)$ shows that E_R is higher by 0.06 eV than E_0. A sharp cut-off at $E = E_R$ corresponds to 0.02 eV. For $e > 0.06$ eV, $N(e)$ decreases with increasing e as expected from the dependence of both j and P on E. The solid curve in figure 9 is the energy distribution calculated by this simple model of $N(e) \propto j P_{\mathrm{LZ}}$ assuming v_R to be proportional to $\sqrt{E - E_R}$ and a constant E_i. It is evident that the phonon-kick model describes well the overall features of the experimentally determined energy distribution of desorbed Si atoms.

3.3. Characteristics of excitation-induced instability on other reconstructed Si surfaces

3.3.1. Si(001)-(2 × 1) *surfaces.* The Si(001)-(2 × 1) surface is also a typical example of a reconstructed Si surface, and is the most technologically important semiconductor surface. The structure of this surface is characterized by the surface-Si dimer with an asymmetric configuration [1], as schematically shown in the inset of figure 10. The formation of asymmetric dimers results in several surface-specific electronic states, as revealed by electron spectroscopic studies. The D_{up} and D_{down} states, associated with dangling bonds of $\mathrm{Si_{up}}$ and $\mathrm{Si_{down}}$ atoms, have been studied extensively, and electronic structures are well understood [1]. Also, there are deeper occupied states consisting of the back-bonds of Si dimers and of σ bonds between Si dimers [1, 49].

A comprehensive study on the excitation-induced instability on this surface has been performed by combining STM and FNRIS [10]. In that study, the surfaces of p-type specimens

[1] The phase-factor correction, which enhances number densities for low velocity particles, yields a translational energy of 0.06 eV, although the peak flight time in experimentally measured TOF spectra corresponds to 0.15 eV.

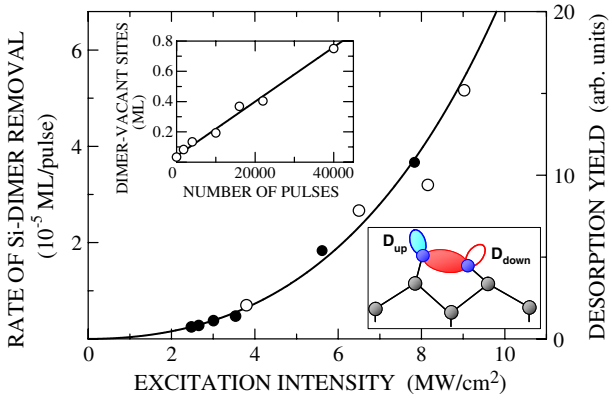

Figure 10. The rate of Si-dimer removal (solid circles) and the yield of atomic Si desorbed from the surface (open circles) as a function of the excitation intensity of 532 nm laser pulses. The inset shows the concentration of dimer-vacant sites as a function of the number of incident 3 ns laser pulses of 532 nm at a fluence of 35 mJ cm^{-2} (after [10]).

were prepared to reduce the concentration of dimer-vacant sites (DVSs) to less than 0.03 ML prior to excitation. They were excited with ns laser pulses at the fluences (Φs) below 100 mJ cm^{-2} and at wavelengths from 700 to 355 nm.

Systematic analysis of STM images of more than 10 000 unit cells showed that the concentration of DVSs increases with increasing dose. In this process of DVS formation, DVSs are generated mostly at perfect (2 × 1) sites for DVS concentration lower than 0.1 ML [10]. Therefore, it is evident, similar to the case of Si(111)-(7 × 7), that the intrinsic surface sites of the (2 × 1) structure are subject to bond rupture, and Si dimers are removed as a whole from the intrinsic site in the bond rupture process. As a typical example of quantitative analysis of DVS formation, we show the growth of DVS as a function of laser-shot number m at a given intensity in the inset of figure 10. It is clear that the concentration increases in proportion to m. The fluence of the 3 ns laser pulse (532 nm) is 35 mJ cm^{-2}, which is far below the melt threshold. The estimated temperature rise at the surface is about 160 °C. Since the dimer structure of the (2 × 1) surface is stable up to 700 K [50], laser-induced heating cannot induce structural changes. Therefore, laser-induced removal of Si dimers is due to an electronic mechanism. In fact, the rate shows a resonant-type dependence on excitation wavelength, characteristic of electronic processes.

Based on the linear relation, the rate K of Si-dimer removal per pulse has been evaluated similar to the case of Si(111)-(7 × 7); it is about 2 × 10^{-5} ML per pulse in this case. The magnitude of K has been determined at different excitation intensities, and at several excitation wavelengths, to reveal wavelength and intensity dependent features. Solid circles in figure 10 show the intensity dependence of K under 532 nm excitation [10]. The removal rate shows super-linear dependence on I_{ex}. Similar results were observed at excitation wavelength from 600 to 355 nm, although the magnitude of the rate was dependent strongly on the excitation wavelength.

In order to have more insight into the process of excitation-induced Si-dimer removal, desorption processes have been studied by applying the FNRIS technique [10]. Although RIS is a powerful technique to probe Si atoms at a selected photon energies, it is not possible to probe simultaneously Si_2 molecules, which could be a candidate for the primary desorbate from this surface. Therefore, we use FNRIS to detect all desorbed neutral species simultaneously.

Similar to the case of Si(111)-(7 × 7), no ionic species were detected at the laser wavelengths and fluences used. Neutral Si atoms and Si_2 molecules were detected at different peak flight times. Therefore, the Si atoms detected are not due to dissociative ionization of Si_2 molecules, but are direct products of surface excitation. The relative ratio of desorbed Si_2 to atomic Si is about 8×10^{-2}, thus the neutral Si atom is the primary product of desorption induced by laser excitation. The peak-flight time of desorbed Si atoms is 0.9 μs, corresponding to a kinetic energy of 0.18 eV, and the shapes of TOF spectra do not depend on laser intensity or on wavelength (from 355 to 650 nm) [10]. These results confirm that desorption of Si atoms is not due to thermal effects, and demonstrate that the final step of the desorption process is the same regardless of excitation intensity or wavelength. In figure 10, the yield of Si atoms desorbed under 532 nm excitation is also plotted (open circles) as a function of I_{ex}, and is compared with the dimer-removal rate evaluated from the STM studies. It is clear that both quantities show the same super-linear dependence on I_{ex}. Therefore, we can conclude that the atomic-Si desorption is a direct consequence of laser-induced dimer removal on this surface. This conclusion implies that the partner of Si dimers is left on the surface after bond rupture. Since monatomic Si atoms adsorbed on Si(001)-(2 × 1) have high mobility at room temperature, they can undergo diffusion to several sinks on the surface. In fact, Si-atom clusters have been detected under intense excitation, where diffusing Si atoms can form adatom clusters on the surface [51].

The super-linearly dependent rate of bond rupture was the case for all excitation wavelengths. However, the Si-desorption yield is strongly dependent on excitation wavelength at a fixed fluence. By introducing a practical desorption efficiency, similar to the case of Si(111)-(7 × 7), excitation-wavelength dependent features of the rate has been examined [10]. It has been found that the efficiency is negligibly low below 1.9 eV, forms a peak at 2.4 eV, and increases again gradually above 2.6 eV. The results indicate first that pure bulk-valence excitation cannot induce the electronic bond rupture on this surface, since photon energies below 1.9 eV are still larger than the bandgap energy (1.12 eV). As discussed in section 3.2.2, none of the bulk optical properties of Si crystals display a peak around 2.4 eV. Alternatively, the surface-reflection spectroscopy has reported two surface-specific transition peaks at 1.5 and 2.4 eV [52]. These bands have been assigned, respectively, to the optical transition from the D_{up} to D_{down} states of the dimers, and to the transition from the back-bond state of Si dimers to D_{up}; the back-bond state located 1.4 eV below the VBM is predicted around the K point [49]. The 2.4 eV peak in the efficiency of Si-atom desorption coincides with the peak at 2.4 eV in the surface reflection spectrum. Therefore, we presume that the surface optical transition plays an important role in the electronic bond rupture on Si(001)-(2 × 1). The important role of the surface optical transition around 2.4 eV on dimer-bond rupture may be proven by STM observation of laser-induced effects on H-terminated Si(001)-(2 × 1), where surface-specific D_{up} and D_{down} states completely disappear by Si–H bond formation. Laser excitation at 532 nm at $\Phi = 200$ mJ cm^{-2} on Si(001)-(2 × 1):H cannot induce any Si-dimer removal, although Si–H bonds can be broken locally by a thermal mechanism [53].

Thus, the features of excitation-induced structural instability on Si(001)-(2 × 1) are similar to those on Si(111)-(7 × 7), although the atomic structures and electronic properties of the two surfaces show significant differences.

3.3.2. Si(111)-(2 × 1) surfaces. The Si(111)-(2 × 1) surface is characterized by quasi-one-dimensional zigzag chains of Si atoms, associated with a substantial buckling [1]. The buckling is accompanied by a net charge transfer from the down (Si_{down}) to up (Si_{up}) atoms of the chain, inducing a significant ionicity in the bonding [1]. A side view of the structure is shown schematically in the inset of figure 11.

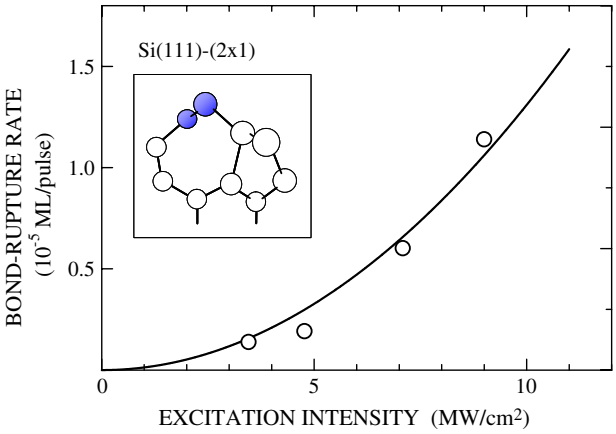

Figure 11. The bond-rupture rate at surfaces with vacancy concentration less than 0.1% as a function of excitation intensity on n-type Si(111)-(2 × 1) surfaces (after [11]). The solid curve is the result of theoretical calculation using the model proposed in [77] (see the text).

The surface-specific electronic structures of this surface have been studied by several spectroscopic methods [1, 54, 55] and theoretical calculations [56–58]. On this surface, the transition from the occupied Si_{up} dangling-bond band (π) to the un-occupied Si_{down} band (π^*) shows a strong peak at 0.45 eV, which is far below the bulk bandgap of 1.12 eV. The transitions at different symmetry points of the surface Brillouin zone take place above 1.3 eV with lower transition strength and with opposite polarization properties [55]. Between the two bands, around 1.2 eV, surface-specific transitions become negligibly weak. Therefore, the primary effect of laser light around 1.2 eV is bulk-valence excitation to generate holes and electrons with small excess energies, the lowest valence excitation.

Systematic studies of the excitation-induced structural instability on this surface have been performed by using mainly STM observation of laser-excited surfaces [11, 59, 60]. It has been shown that Si_{up} atoms at intrinsic sites are subject to electronic bond rupture under excitation at 1.16 eV. Figure 11 shows the rate of bond rupture, at perfect surface sites, as a function of the excitation intensity of 3 ns laser pulses at 1.16 eV [11]. The rate depends super-linearly on excitation intensity, thus showing one of the common features of excitation induced instability. Studies have been extended to a wider excitation-wavelength range from 1.16 to 3 eV, to confirm that laser excitation induces Si-atom removal with a similar intensity dependence of the bond-rupture rate [60].

However, we emphasize a few remarkable differences in characteristics observed on this surface from those on Si(111)-(7 × 7). The first is the role of bulk-valence excitation. On Si(111)-(2 × 1), the surface bond rupture to remove threefold-coordinated Si_{up} atoms is induced by 1.16 eV excitation. As mentioned above, valence excitation dominates over the surface-specific transitions around 1.2 eV. Therefore, the result in figure 11 shows clearly that bulk-valence excitation induces electronic bond rupture of atoms at the intrinsic surface site for the Si(111)-(2 × 1) surface. This feature shows a strong contrast to those on Si(111)-(7 × 7) and Si(001)-(2 × 1) described above.

The second difference is concerned with the morphology of surface structural changes. Figure 12 shows STM images acquired prior to, (a), and after, (b) and (c), irradiation with laser pulses at a fluence of 32 mJ cm^{-2} [11]. In the images, each white spot corresponds to Si_{up}. Single-domain terraces, as wide as 0.4×0.4 μm^2, include a very small defect concentration less than 10^{-3} ML prior to laser irradiation. On the other hand, we evidently see several dark spots newly generated after laser excitation in figures 12(b) and (c). The dark spots are vacancies formed by bond rupture of top-most Si_{up} atoms on the surface. By comparing the two images at exactly the same spot on the surface but irradiated with different doses, figures 12(b) and

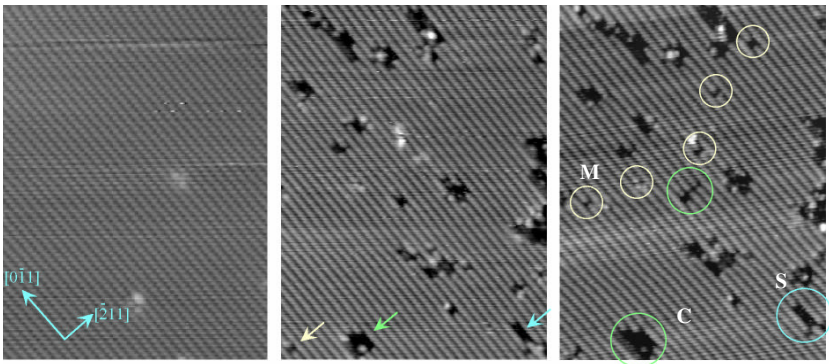

(a) before excitation (b) after 5000 shots (c) after 20000 shots

Figure 12. STM images of Si(111)-(2 × 1) prior to, (a), and after, (b) and (c), laser irradiation acquired with a negative sample bias of −2.5 V. Images (b) and (c) represent structures at the same spot of the surface, but irradiated with 5000 and 20 000 shots of 1064 nm laser pulses at a fluence of 32 mJ cm^{-2}. White circles in (c) show the sites where monovacancies are newly generated, while green circles show the vacancy clusters, the sizes of which increase by bond rupture at sites nearest to pre-existing vacancies.

(c), we find precisely different modes of vacancy formation. At the sites enclosed by circles labelled M the monovacancies (V_M s) are newly generated at originally perfect Si_{up} sites, while at the sites shown by circles C large vacancy clusters have been generated via bond rupture at sites nearest to pre-existing vacancies. Quantitative analysis has shown that the rate of bond rupture at sites nearest to pre-existing vacancies is more than 100 times greater than that at perfect sites [60]. Consequently, vacancy clusters are formed efficiently on Si(111)-(2 × 1). On the other hand, bond-rupture events take place randomly up to a vacancy level of 0.06 ML on Si(111)-(7 × 7). Therefore, some surface-dependent characteristics lead to the striking difference in the morphology of structural changes resulting from the excitation-induced instability. As a cautious note, we emphasize that the differences in the morphology are not related to any properties originating from the metastability of this surface. As described in the next section, other reconstructed surfaces with stable configurations show essentially the same features as those of Si(111)-(2 × 1). We will discuss the origin of the different morphologies in the last section from a unified point of view for the excitation-induced structural instability.

4. Excitation-induced structural instability on InP(110)-(1 × 1)

The {110} surface of compound semiconductors with cubic zinc-blende structure is well studied, and electronic and structural properties are known in detail [1]. Although no reconstructions like Si surfaces are induced, the surface atoms of the same number of metallic (cation) and nonmetallic (anion) atoms are relaxed from the positions expected for a bulk-like termination, such that the cation–anion zigzag chains become tilted with the anions being raised. This relaxation, associated with charge transfer from cations to anions, characterizes surface-specific electronic states; the highest occupied surface state (S_1) is composed of s-like dangling bonds of anions located below the valence-band maximum (VBM) and the lowest unoccupied surface state is composed of p-like dangling bonds of cations located above the conduction-band minimum (CBM) [1]. There are no intrinsic surface states within the bandgap (although GaP is a possible exception).

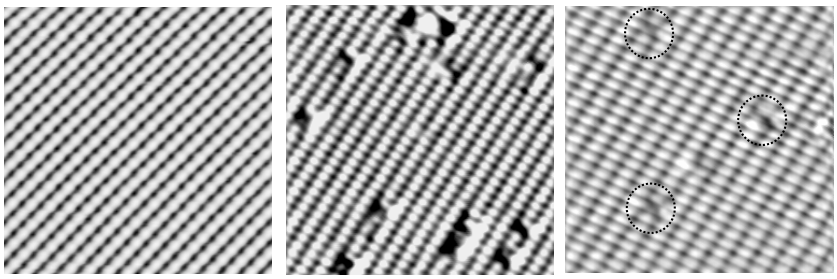

Figure 13. STM images of In(110)-(1 × 1) before, (a), and after, (b) and (c), irradiation with 460 nm laser pulses at 2.8 mJ cm^{-2}. P atomic images were acquired with a negative sample-bias of −2.3 V in (a) and (b), and the In atomic image with a positive voltage of +2.5 V in (c) (after [12]). Broken circles in (c) show the sites where In vacancies are formed.

Several laser-stimulated desorption studies have been performed on III–V semiconductor surfaces, although the results are controversial. The controversy is due partly to the low sublimation energies of these surfaces. Since laser-induced heating plays some role even well below the surface melting temperature [61], clear demonstration of electronically induced processes is not straightforward. Also, strong activities of surface defects under photoexcitation [2, 8, 25] prevent us from unambiguous observation of intrinsic surface processes. Although an inherent instability of surface metallic atoms under valence excitation was suggested theoretically for III–V semiconductor surfaces [62, 63], experimental examination of the predicted instability was not possible until recently. Similar to the case of Si surfaces, use of STM to observe direct atomic imaging of laser-excited III–V semiconductor surfaces has opened a new level of research. The first STM study of laser-irradiated InP(110)-(1 × 1) demonstrated the formation of vacancies at P atomic surface sites under ns laser excitation by an electronic mechanism [64]. On the other hand, Ham *et al* claimed that ns laser irradiation did not induce surface bond rupture, although low-energy electron irradiation did generate vacancies at surface anion sites on GaAs(110)-(1 × 1) [8]. Therefore, even the role of valence excitation in the intrinsic structural instability on III–V semiconductor surfaces remained an open question for several years.

The present authors have undertaken comprehensive studies on the laser-induced structural instability on III–V semiconductor surfaces, by combining both STM and FNRIS results [12]. The combined results demonstrate that intrinsic structural instability is induced on InP and GaAs(110)-(1 × 1) surfaces under bulk-valence excitation, with a prominent species-sensitive bond rupture rate. However, the inherent instability of metallic atoms predicted theoretically is not found; in fact, non-metallic atoms are preferentially removed from surfaces.

4.1. Electronic bond rupture at intrinsic surface sites: species dependence

As in the case of Si surfaces, direct atomic imaging of laser-excited surfaces gives fundamental information on the structural changes induced by the excitation. In order to detect intrinsic processes of excitation-induced instability, and to identify unambiguously the consequences of the instability, the surfaces were prepared carefully to reduce surface-defect concentrations prior to laser excitation. As a typical example, we show, in figure 13, STM images of an n-type InP surface acquired before, (a), and after, (b) and (c), irradiation with 460 nm laser pulses at a fluence of 2.8 mJ cm^{-2} [12]. Images (a) and (b) represent P atomic images, while image (c) shows the In atomic image. As seen in image (a), the surfaces prior to irradiation have very few

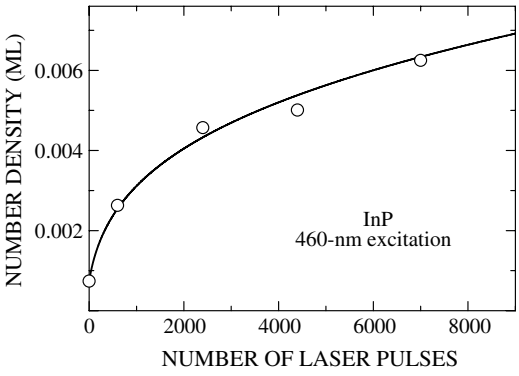

Figure 14. Growth of the total number density of P vacancies as a function of the number of incident 460 nm laser pulses (5 ns width) at 4.5 mJ cm^{-2} (after [12]). The solid curve is the result of theoretical calculation by using the model proposed in [77] (see the text).

surface defects (less than 0.001 ML), mostly in the form of monovacancies at P and In atomic sites. In fact, we could not see any such defects in this size of image. On the other hand, laser excitation induces several dark spots newly generated at both P and In sites, as seen in images (b) and (c). The dark spots have been identified as vacancies formed at P and In sites, based on the quantitative correlations between these dark spots and P and In atoms desorbed from the surface, as will be described below. Dual-bias imaging for the same spot on the surface revealed that there were no spatial correlations between monovacancy sites of P and In atoms. Therefore, removal of P and In atoms takes place as a separate event to generate monovacancies at respective sites.

In image (b), P vacancies take the form of monovacancies and vacancy clusters, while In vacancies are mostly monovacancies as seen in image (c). Statistical analysis, of the images surveyed over 50 000 surface sites, showed that monovacancies were generated predominantly in low dose regions and that larger P-vacancy clusters grew progressively at higher doses. Therefore, the primary step is the bond rupture at originally perfect sites to generate monovacancies. Vacancy clusters are formed subsequently by bond rupture at sites near existing monovacancies. This feature of efficient formation of P-vacancy clusters is similar to the case of Si(111)-(2 $\times$ 1) in section 3.3.2, but contrasts strongly with the case of exclusive monovacancy formation on Si(111)-(7 $\times$ 7). We leave this interesting result as a subject of later discussions and we focus our attention here on bond-rupture process at perfect surface sites. Although bond breaking at originally perfect sites and at sites near pre-existing defect sites takes place within the exciting laser pulse, we can evaluate unambiguously the rate of the former process by introducing two different quantities for vacancies [12]. In the statistical analysis of the growth of vacancies, we introduce the number density N_j and the vacancy-site density V_j for a vacancy cluster consisting of j vacancy sites. N_j is registered simply as a count of vacancy clusters, irrespective of their size. V_j is registered as j, the number of sites, in an individual vacancy cluster. Any bond ruptures at sites nearest pre-existing vacancies enhance the magnitude of the total vacancy-site density V ($=\sum_j V_j$), but do not change the total number density N ($=\sum_j N_j$). Therefore, N represents purely the concentration of new vacancies formed at originally perfect sites, free from vacancy formation near pre-existing defect sites. In figure 14, we show N for P vacancies as a function of number of incident laser pulses at the intensity of 0.9 MW cm^{-2}. The total number density increases far above that detected prior to laser irradiation, thus demonstrating unambiguously that laser-induced vacancy formation takes place at perfect P sites.

Desorption upon excitation of the surfaces with ns laser pulses has been studied by means of FNRIS [12]. A typical mass spectrum detected by FNRIS is shown in the inset of

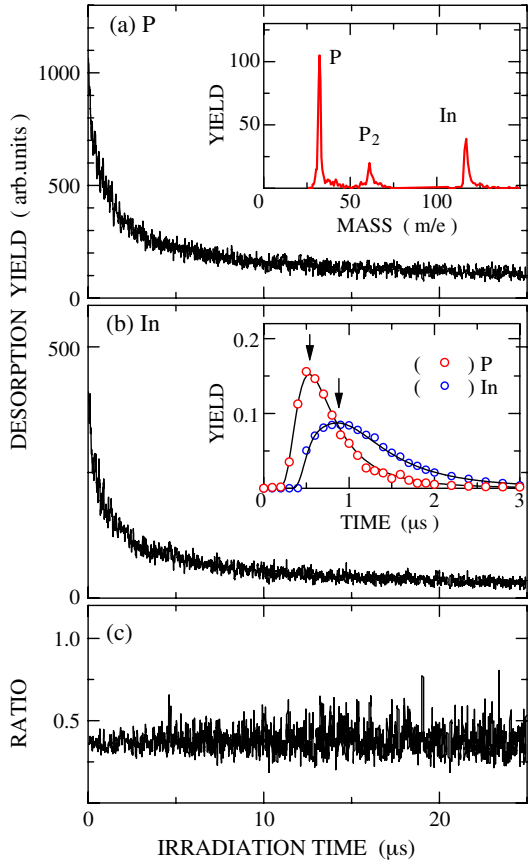

Figure 15. Desorption yields of P atoms, (a), and In atoms, (b), and the ratio of the yield of In relative to that of P atoms, (c), as a function of irradiation time of 460 nm laser pulses. The inset of (a) shows the mass spectrum of neutral desorbed species, and the inset of (b) shows the time-of-flight spectra of P and In atoms (after [12]).

figure 15(a). Three different neutral species were detected in the spectra; these were monatomic P, diatomic P_2 and monatomic In. Monatomic P is the major desorbed species with the yield higher than the In yield. InP molecules were not detected, and no ions were emitted. Figures 15(a) and (b) show the desorption yield of P and In, measured simultaneously as a function of irradiation time t, which is defined as the product of pulse width (5 ns) and number m of laser shots incident on the surface. The yields of both species are reduced significantly with increasing t. This reduction of desorption yield again shows a strong contrast to the case of Si(111)-(7 × 7), where the yield is constant under repeated irradiation at a fixed fluence of laser pulses. An important finding is that the yield of In relative to that of P remains constant irrespective of the sharp drop in total yield during irradiation as shown in figure 15(c). This result suggests that the same mechanism induces desorption of both species.

Velocities of P and In atoms were measured by changing time delay between the excitation and probe pulses. The TOF spectra, inset to figure 15(b), are characterized by the peak flight times of 0.6 and 1.0 μs, which correspond to kinetic energies of 0.2 and 0.3 eV, respectively. The different flight times of P and In atoms exclude the possibility of dissociative ionization of desorbed InP molecules, and show clearly that these atoms desorb separately, consistent with the STM observation that monovacancies at P and In sites are formed during separate events. The yield of desorption has been correlated quantitatively with the total vacancy-site density V. For the bond-rupture rate $g(t)$ at time t, the desorption yield is proportional to $g(t)$, while V is given by the integral of $g(t)$ over t. Then, we compare the time-integrated yield $Y(t)$ (solid

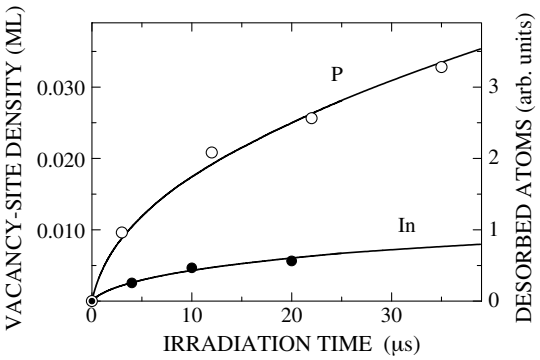

Figure 16. Growth of total vacancy-site densities of P and In vacancies upon excitation by 460 nm laser pulses. The solid curves are the time-integrated desorption yields of P and In atoms measured simultaneously by FNRIS (after [12]).

curves) with V in figure 16 for P and In atoms. It is evident that these two quantities show essentially the same dependence on t. Therefore, desorption is the direct consequence of the bond rupture of P and In atoms on the surface.

It has been reported that P monovacancies can be formed thermally on InP(110)-(1 × 1) [65, 66]. The rate of this thermal process is significantly higher on p-type surfaces than n-type surfaces, showing an interesting Fermi-level effect. The rate of this thermal process is negligible at 296 K even on p-type surfaces. However, one may argue that a possible temperature rise ΔT by laser heating might enhance the rate even on our n-type surfaces. The ΔT upon ns laser irradiation, estimated from the standard formula of laser heating [25], is less than 30 K even at the maximum fluence of 5 mJ cm^{-2}. At the estimated highest temperature (326 K), a rate of about 1.3×10^{-7} ML s^{-1} can be interpolated from published data for p-type InP [65], which is too low to account for the P vacancies formed by laser excitation. Therefore, it is concluded that the bond rupture induced by laser excitation is not due to laser-induced heating. This conclusion is substantiated definitively by the FNRIS results. It has been shown that desorbed neutral atoms and molecules have the kinetic energies corresponding to the surface temperature in the case of desorption due to the laser-induced heating process [16, 61]. For example, a surface temperature of about 400 K has been deduced for GaAs under 532 nm laser irradiation at fluence of 80 mJ cm^{-2} [61]. On the other hand, as shown in the inset of figure 16(b), kinetic energies as high as 0.2 eV, corresponding to a temperature greater than 2000 K, is imparted to P and In atoms under excitation at fluence less than 5 mJ cm^{-2}. Therefore, the desorption is not due to a thermal mechanism, but is due to electronic processes following laser excitation.

In order to study the characteristics of monovacancy formation on pristine surfaces, the desorption has been examined only for *the first* few hundred ns, thus avoiding any contributions from bond rupture near pre-existing vacancies [12]. In the inset of figure 17, we show $Y(t)$ of P atoms as a function of t in this initial region. For any curves measured at different excitation intensities I_{ex}, Y increases linearly until a certain critical value of Y, above which the growth rates start to decrease. The slope of the initial part can be taken as $g(0)$ at perfect sites on the surfaces with low pre-existing defect concentrations. The rate thus determined is plotted (open circles) as a function of I_{ex} in figure 17; it depends super-linearly on I_{ex}. The bond-rupture rate of In, determined by a similar analysis, shows a similar nonlinear feature.

As a specific feature of the surface consisting of binary constituent atoms, the bond rupture shows a strong species-dependent rate. As seen in figure 17, the rates of bond rupture for P and In sites show essentially the same super-linear dependence on I_{ex}. Also, as seen in figure 15, the relative ratio of the yields of desorption of two species is kept constant, irrespective of the rates changing with t. These results suggest that bond rupture of P and In atoms on the

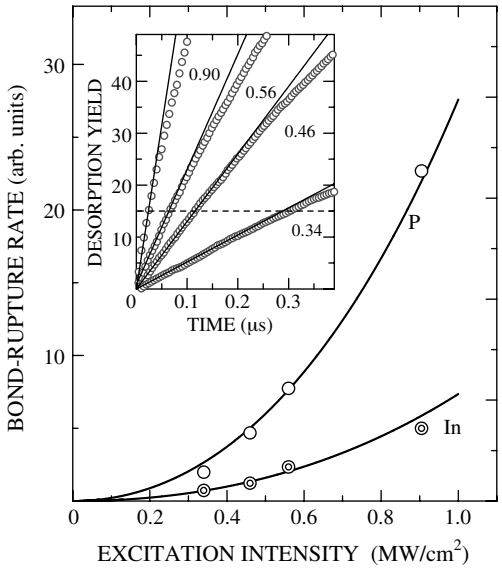

Figure 17. The bond-rupture rate of P and In atoms as a function of excitation intensity of 460 nm laser light. The inset shows the time-integrated yields of desorbed P atoms as a function of irradiation time for four different excitation intensities (after [12]).

surface is induced by the same mechanism, but with a different efficiency, or branching ratio. Desorption results and STM results indicate the efficiency of P-bond rupture is about three times higher than that of In-bond rupture. This result has shown that the theoretical prediction of inherent instability of metallic-atom sites on III–V semiconductor surfaces [62, 63] is not the case.

The essential features of the electronic process described above are the case for broader excitation-wavelength range from 580 to 420 nm, where laser irradiation results mainly in the valence excitation of InP. For this surface, surface differential spectroscopy and polarization-modulated spectroscopy reveal a surface optical transition around 2.7 eV [1, 67, 68], which corresponds to 460 nm. However, excitation using photon energies far from the surface transition results in similar electronic bond ruptures with almost the same efficiency. Therefore, it is evident that the intrinsic structural instability on InP(110)-(1 × 1) is induced by bulk-valence excitation, similar to the case of Si(111)-(2 × 1). Also, the instability is characterized by the local bond rupture at perfect surface sites, followed by subsequent and efficient bond rupture near vacancies, leading to the formation of vacancy clusters. This morphology of surface-structural change is also the same as that on Si(111)-(2 × 1).

4.2. Fermi-level dependent morphology of surface defects formed by laser-induced electronic bond breaking: Identification of excited species responsible for the bond rupture

One of the key issues to elucidate the mechanism of the instability is the identification of electronic excited species responsible for structural changes (the reactive species hereafter). Laser irradiation can excite both surface and bulk electronic states, and generate electrons, holes, excitons, and even electron–hole plasma under intense excitation. The roles of these excited species in the instability have not been clarified yet, although a few models have been proposed [9, 62, 63]. Although previous studies have suggested an important role of the valence holes [3, 6, 7, 10–12], the conclusions are still circumstantial; more definite and direct results to identify the reactive species are highly desirable to deepen fundamental understanding of the mechanism.

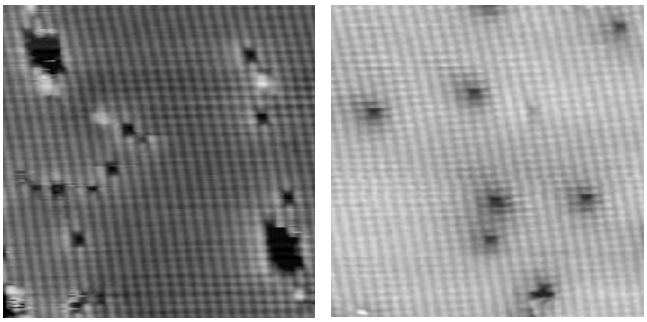

(a) (b)

Figure 18. STM images of InP(110)-(1 × 1) after laser irradiation. The images (a) and (b) represent, respectively, the P atomic structures on n- and p-type surfaces Laser irradiated with 5000 shots of 3 ns laser pulses at 460 nm with fluence of 2.8 mJ cm^{-2} (after [70]).

The {110) surfaces of most III–V compound semiconductors are unique in that there are no intrinsic surface electronic states in the bandgap [1]. Therefore, the band maintains flat-band condition even under optical excitation. However, once surface vacancies are formed at non-metallic atom sites, the vacancies introduce charge transfer levels. Consequently, they are charged positively or negatively, depending on the Fermi level of particular specimens, and induce local band bending around them [69]. Therefore, they can act as *a local marker* for carrier localization on surface sites, when carrier localization is essential in the electronic bond rupture. On the other hand, when exciton localization is important, then charges at vacancy sites with either polarity will not play any significant role because of charge neutrality of excitons. Based on the consideration above, Fermi-level dependent morphology of surface vacancies formed upon laser excitation has been studied in detail for InP(110)-(1 × 1) by direct imaging of irradiated surfaces by STM [70]. The results demonstrate unambiguously that the reactive species responsible for the electronic bond rupture are the valence holes generated by laser excitation.

Figure 18 presents STM images acquired with a negative sample-bias voltage after laser excitation of (a) n-type and (b) p-type surfaces [70]. Both surfaces were excited with 3 ns laser pulses (460 nm) at the same excitation intensity and dose. On surfaces prior to irradiation, concentrations of surface defects were less than 10^{-3} ML as before (see figure 13). On the other hand, figure 18 shows that P-atomic vacancies (V_P s) are newly generated after laser excitation. However, the morphology exhibits a remarkable difference. On n-type surfaces, the V_P are mostly in the form of vacancy clusters: vacancy strings in which adjacent P atoms are removed along a chain one dimensionally, and vacancy islands where the V_P are clustered across the chains two dimensionally. In contrast with this feature of n-type surfaces, the V_P on p-type surfaces are mostly in the form of monovacancies, as seen in figure 18(b).

The difference in morphology is not specific to the pair of images shown in figure 18. Images surveyed over 50 000 unit cells on irradiated surfaces were analysed statistically to classify the vacancies into two groups: monovacancy and vacancy cluster. The histograms of figure 19 show the result of this analysis for n- and p-type surfaces; results on the surfaces irradiated with several shots of incident laser pulses are compared. As clearly seen in the figure, vacancy clusters are formed predominantly on n-type surfaces, whereas monovacancies are generated almost exclusively on p-type surfaces. Essentially the same results have been obtained for GaAs(110)-(1 × 1) [70].

As described above, anion monovacancies are positively (negatively) charged on p-type (n-type) (110) surfaces [69]. Since the net charge of monovacancies is unity for both n- and p-type

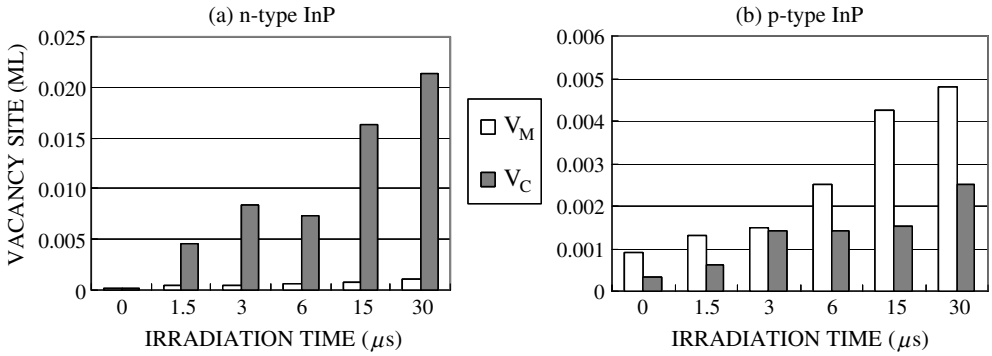

Figure 19. A histogram of the vacancy sites in the form of monovacancy, V_M, and vacancy cluster, V_C, on n-type, (a), and p-type, (b), surfaces irradiated with laser pulses at a constant intensity (0.93 MW cm^{-2}). The sites in V_M and V_C are plotted as a function of number of incident laser pulses (after [70]).

surfaces, their repulsive interaction is essentially the same. Therefore, the striking difference in morphology of structural changes between p- and n-type surfaces cannot be due to any effects of re-distribution of vacancies after their generation with similar spatial distribution. The difference in morphology results directly from some primary processes of bond rupture of surface atoms upon photoexcitation.

As shown in section 4.1, the electronic bond rupture at perfect surface sites to form monovacancies is the primary step. Once monovacancies are formed, the defect sites may provide efficient localization sites for mobile excited species, due to charging effects, rupture of translational symmetry, and formation of localized electronic states. Also, atoms near pre-existing vacancies are in weakened-bond configurations [71], with possible enhanced efficiency of bond rupture. Therefore, general consideration predicts efficient clustering of vacancies under electronic excitation, *unless localization of reactive species is prohibited around the vacancies*. The vacancy clustering is certainly the case on n-type surfaces, but not on p-type surfaces. Therefore, on p-type surfaces, the reactive species is prevented from localization at sites near the pre-existing vacancies by some mechanism.

The local band bending due to charged anion vacancies results in the condensation, or in the exclusion, of carriers via their Coulomb-type interaction. The finding of remarkable Fermi-level dependent morphology indicates clearly that the upward band bending due to a negatively charged vacancy on n-type surfaces leads to the condensation of the reactive species, but that the downward bending due to a positively charged vacancy on p-type surfaces prevents the species from localization around the vacancy. Evidently, the valence hole is the only entity that satisfies this requirement. Therefore, we conclude that valence-hole localization at surface sites is essential for the electronic bond rupture on III–V semiconductor surfaces.

Here, it is worthy of mention that crucial roles of the valence holes in surface bond rupture on (110) surfaces of III–V semiconductors have been evidenced by an interesting electronic effect on spontaneous formation of the anion monovacancies on p-type surfaces at room temperature. Semmler *et al* have shown that the formation rate is enhanced significantly for higher p-doping [66], which enhances the density of valence holes *injected chemically*. Also, the morphology of the anion vacancies formed on p-type surfaces is characterized by exclusive monovacancy formation. This morphology is also consistent with our conclusion that the reactive species is the valence hole, since localization of holes near pre-existing positively charged vacancies is prevented.

5. A proposed mechanism of the excitation-induced instability on semiconductor surfaces

5.1. Summary of experimental results and issues to be solved

As described in the previous sections, the electronic process of bond rupture at intrinsic surface sites on covalent semiconductor surfaces shows some important common features. First, atoms at perfect surface sites are subject to bond rupture, thus demonstrating the intrinsic nature of the processes. Second, the rate of bond rupture shows super-linear dependence on the excitation intensity of laser light for photon energies between 1 and 4 eV. Third, the rate of bond rupture depends sensitively on the type of surface site and atomic species.

However, there are two qualitatively different features that separate the surveyed surfaces into two groups. For the first group, Si(111)-(7 × 7) and Si(001)-(2 × 1), the rate of bond rupture shows a strong excitation-wavelength dependence as shown in figure 5. It appears that the instability for this group needs specific surface-optical transitions. On the other hand, there is no significant wavelength dependence of the bond-rupture rate for the second group, InP(110)-(1 × 1) and Si(111)-(2 × 1). The instability on these surfaces can be induced by a broad wavelength range that is known to induce bulk-valence excitation. The second distinguishing feature is evident in the morphology of surface-structural changes induced by excitation. In the first group of Si(111)-(7 × 7) and Si(001)-(2 × 1), bond-rupture processes take place randomly, without any spatial correlations among vacancy sites. On the other hand, efficient bond rupture at sites near pre-existing vacancies is induced, leading to efficient formation of vacancy clusters, in the second group of Si(111)-(2 × 1) and InP(110)-(1 × 1). Any physical mechanism for the instability should describe consistently all of the common features and substantial differences depending on surface properties.

Since the excitation-induced instability is surface specific, it is clear that charge redistribution on surfaces, induced by generation and relaxation of surface excited states, plays crucial roles in the instability. Surface excited species can be populated by two different channels: direct surface-specific optical excitation, and indirect electronic excitation transfer from bulk to surface states. Since optical-transition energies between surface electronic states are overlapped with those of bulk-electronic states, in most cases [1], both channels can be active under excitation at a given photon energy. However, because of the small absorption coefficient of the surface [54], most photoexcitation occurs in the bulk valence system, where electron–hole pairs are generated with a high density. The dense valence excitation, typically 10^{19} cm^{-3}, can transfer to the surface electronic system through electron–phonon and/or electron–electron scattering [72], leading to surface structural changes and desorption of constituent atoms. In fact, the results for InP(110)-(1 × 1) and Si(111)-(2 × 1) have shown clearly that bulk-valence excitation induces electronic bond rupture of surface atoms at intrinsic sites. Therefore, quantitative examination of the effects of bulk-valence excitation on surface bond rupture is primarily important for understanding the mechanism of this surface-specific phenomenon.

As described in section 4.2, extensive studies on InP surfaces have shown unambiguously the crucial role of holes injected into the surface electronic states. Therefore, we focus our attention here on the role of laser-generated valence holes. Sumi studied theoretically the effects of densely populated valence holes on electronic bond rupture on semiconductor surfaces, and found localization of two holes (two-hole localization, THL), at the same surface bond, to be important [62]. Although the two-hole (or multi-hole) mechanism has been widely used to describe ion desorption induced by core–hole excitation on ionic surfaces [73, 74], the mechanistic processes of THL by Sumi are significantly different from those in ion-desorption processes. The primary mechanistic assumption is that surface bond rupture leading

to neutral-atomic desorption (not ion desorption) can be induced by strong lattice relaxations associated with localization of two valence holes on the same surface bond [18, 62]. This assumption is based on the Anderson negative U concept: that the localization of two carriers with the same charge is possible when strong lattice coupling results in favourable system energetics [75]. The negative U interaction of two-hole localized configurations corresponds to the displacement of surface atoms into the vacuum in the THL mechanism. Thus, together with the Coulomb interaction energy U and the valence bandwidth B, which are important to give an energy relationship in the two-hole mechanism for the ion-desorption mechanism [73, 74], the electron–lattice interaction S becomes a crucial physical quantity that characterizes the energy relationship in the THL mechanism.

Sumi has formulated the rate of successive localization of two holes on a surface bond for a thermally equilibrated valence system. Based on the general formula of the THL rate, he derived a conventional analytical rate expression for equilibrated valence holes confined two dimensionally within the surface region. However, valence excitation can induce surface bond rupture for the cases not considered in Sumi's theory. For example, InP and GaAs(110)-(1×1) surfaces have no intrinsic surface states in the gap, and maintain a flat-band condition under excitation [1]. Recent surface carrier dynamics studies indicate that p-type Si(001)-(2×1) also maintains a flat-band condition when excited [76]. Under the flat-band condition, laser-light excitation with photon energies larger than the bandgap energy leads to a dense population of valence holes and conduction electrons. The electrons and holes thus formed show strong non-equilibrium features of diffusion caused by high concentration and temperature gradients. Therefore, instead of forming equilibrated two dimensionally confined valence holes assumed in Sumi's theory, non-equilibrium three-dimensional electron–hole pairs are generated by optical excitation.

In the more general cases, band bending of semiconductor surfaces may act to confine carriers in the surface region. For surfaces of n-type crystals, upward band bending may form two dimensionally confined valence holes. However, a finite band bending due to Fermi-level pinning can easily be reduced using the surface photovoltaic effect to establish flat-band conditions under dense excitation [1]. Photoelectron spectroscopy studies have shown that the temporal change of the photovoltaic effect is very fast, and takes place within at least a few ps after excitation for Si surfaces [77]. The band, flattened under dense excitation, remains flat for microseconds [78]. Therefore, most photogenerated carriers are governed by flat-band conditions shortly after ns laser excitation to form a non-equilibrium three-dimensional excitation.

Theoretical examination of the THL mechanism for densely populated non-equilibrium valence holes with three-dimensional character, which was beyond the theoretical consideration by Sumi, has been made recently [79]. Below, we first describe the theoretical modelling. After demonstrating the validity of the theory through quantitative analysis of typical results of InP(110)-(1×1) and Si(111)-(2×1), we investigate possible reasons why bulk valence excitation is not active for inducing the instability on Si(111)-(7×7) and Si(001)-(2×1) in the light of the model. Then, based on the critical examinations, we construct a unified model that can describe systematically not only the super-linear dependence of the bond-rupture rate on the excitation intensity, but also the significant differences in wavelength-dependent features and in the morphology of surface-structural changes.

5.2. The rate of two-hole localization for non-equilibrium valence excitation

Efficient carrier diffusion can dominate non-equilibrium dynamics of photogenerated electron–hole populations in semiconductors. Densely populated carrier dynamics has been investigated

extensively in semiconductor laser annealing studies. Based on the standard concept of quasi-equilibrium in carrier transport [80], quasi-Fermi levels of electrons (ψ_e) and holes (ψ_h) and an effective temperature T^* were used to describe local carrier distributions for temporal domains longer than a few ps after optical excitation [81, 82]. Later studies of hot carrier dynamics in semiconductors and on their surfaces in short temporal domains have confirmed that the electronic quasi-equilibrium is established within 1 ps of fs-pulse excitation [83, 84]. Then, under the effective-mass approximation, the quasi-equilibrium local carrier concentrations N_c ($c = \mathrm{e}$ for electrons and $c = \mathrm{h}$ for holes) at position $\vec{r}$ and time t of a three-dimensional valence system is given by

$$N_c(\vec{r}, t) = \frac{2}{\sqrt{\pi}} Z_c(T^*) \int_0^\infty \frac{\sqrt{x}}{\exp\{x - \eta_c(\vec{r}, t)\} + 1} \, \mathrm{d}x, \tag{2}$$

where $Z_c(T^*)$ is the effective density of state at effective temperature T^*, and η_c is the reduced quasi-Fermi level, for electrons and holes, given by

$$\eta_\mathrm{e} = \frac{\psi_\mathrm{e} - E_\mathrm{C}}{k_\mathrm{B} T^*}, \qquad \eta_\mathrm{h} = \frac{E_\mathrm{V} - \psi_\mathrm{h}}{k_\mathrm{B} T^*}. \tag{3}$$

The symbols E_C and E_V represent the energies of the CBM and VBM, and k_B is the Boltzmann constant.

Based on the classical Boltzmann equation in the relaxation-time approximation for non-equilibrium thermodynamics, von Driel [82] has shown that the current $\vec{J}$ of pair concentration due to a strong Dember field (under the assumption $\vec{J} = \vec{J}_\mathrm{h} = -\vec{J}_\mathrm{e}$) is given by

$$\vec{J} = -D \left\{ \nabla N + \frac{N}{T^*} \left(\frac{\hat{B}}{\hat{A}} - \frac{3}{2} \right) \nabla T^* + \frac{N}{2kT^*} \frac{1}{\hat{A}} \nabla E_g \right\}, \tag{4}$$

where $\hat{A}$ and $\hat{B}$ are given by

$$\hat{A} = \frac{F^\mathrm{e}_{1/2}}{F^\mathrm{e}_{-1/2}} + \frac{F^\mathrm{h}_{1/2}}{F^\mathrm{h}_{-1/2}}, \qquad \hat{B} = \frac{F^\mathrm{e}_1}{F^\mathrm{e}_0} + \frac{F^\mathrm{h}_1}{F^\mathrm{h}_0}. \tag{5}$$

Here, F^c_j denotes the Fermi–Dirac integral of order j for the carriers, and D designates the ambipolar diffusion constant for excess carriers defined by

$$D = \frac{2k_\mathrm{B} T^*}{e_0} \frac{\mu_\mathrm{e} \mu_\mathrm{h}}{\mu_\mathrm{e} + \mu_\mathrm{h}} \hat{A}. \tag{6}$$

The symbols μ_c and e_0 represent the carrier mobility and unit charge, respectively. Therefore, under dense-excitation conditions, the pair-concentration flow is governed by the density-dependent diffusion constant D, the concentration gradient, the temperature gradient, and the bandgap gradient ∇E_G.

In terms of $\vec{J}$ of equation (4), the local density of carriers is governed by the equation of particle balance, given by

$$\frac{\partial N(\vec{r}, t)}{\partial t} + \nabla \cdot \vec{J} = G(\vec{r}) - R(\vec{r}) \tag{7}$$

where G and R are the pair generation and recombination rates [82]. By solving equation (7) under appropriate boundary conditions, we can evaluate the density of valence holes at the sub-surface layer, which corresponds to the hole density for two-hole localization in Sumi's theory.

For the process of successive localization of two holes at the same site on surfaces, the rate J of forming a two-hole localized state is given by

$$J = N_\mathrm{d} R_\mathrm{SHL}, \tag{8}$$

where N_d is the density of bonds localizing the first hole, and R_{SHL} is the rate constant for localizing a second hole at the same bond. Sumi formulated these two factors for equilibrated electron–lattice systems [62]. For the first-hole localized metastable state with energy E_d (measured from the VBM), N_d is governed by the Fermi distribution function with the Fermi energy E_F. In the case where E_d is larger than E_F to satisfy the condition $\exp\{(E_d - E_F)/k_BT\} \gg 1$, N_d is approximated as

$$N_d = N_0 \exp\{-(E_d - E_F)/k_BT\}, \tag{9}$$

where N_0 represents the total density of surface bonds capable of holding the first localized hole. The rate constant R_{SHL} is approximated by

$$R_{SHL} \approx C \exp(E_F/k_BT). \tag{10}$$

The constant C is specific to the system under consideration and is defined as

$$C = [4\pi/(\hbar^2 S k_B T)]^{1/2} \int dE g(E) \exp[-E/k_BT - (E_b + U - E)^2/(4Sk_BT)]. \tag{11}$$

In equation (11), S represents the lattice-relaxation energy associated with the second hole localization, U is the Coulomb repulsive energy between the two holes localized on a single bond, and E_b is the kinetic energy lost in the process of localizing the second hole at the bond. All these parameters are material and surface specific. Equation (10) is valid when the average kinetic energy E_T of free holes, that tunnel most frequently to one of the first-hole localized bonds, satisfies the condition that $E_F < E_T \ll U$ [62]. The energy E_T is given by

$$E_T = (2\pi k_B T S/\Delta)^{2/3} A^{1/3}, \tag{12}$$

with

$$\Delta = 2S - E_b - U + \tfrac{8}{3}(A/U)^{1/2} S k_B T/U, \tag{13}$$

and

$$A = e_0^4 m_h/(2\varepsilon_s^2 \hbar^2), \tag{14}$$

where m_h is the effective mass of free holes, and ε_s is the static dielectric constant at the surface.

Then, J is given by

$$J = N_0 C \exp(-E_d/k_BT) \exp(2E_F/k_BT). \tag{15}$$

As seen in equation (15), J depends on the excitation density through the factor $\exp(2E_F/k_BT)$, since the Fermi energy governs not only the hole distribution but also the transition rate of the second hole localization against the Coulomb barrier due to the localized first hole.

For three-dimensional dense valence excitations associated with strong carrier diffusion, the Fermi energy is no longer the quantity that characterizes the hole statistics and dynamics, but the quasi-Fermi level ψ_h (or η_h) is the quantity as shown above. Under the presumption of local equilibrium, the Fermi energy E_F, for equilibrated electronic systems, can be replaced by the quasi-Fermi level of valence holes near the surface. Then, under the restriction $\psi_h < E_T \ll U$, equation (10) (valid for equilibrated valence holes) becomes

$$J = J_0 \exp(2\eta_h(0)), \tag{16}$$

valid for non-equilibrated three-dimensional valence holes, where J_0 is defined here as

$$J_0 \equiv N_0 C \exp(-E_d/k_BT^*), \tag{17}$$

and $\eta_h(0)$ represents the reduced quasi-Fermi level of the sub-surface layer ($\vec{r} = 0$). When we take $N(0, t)$ of the solution of equation (7) as the local hole density in the sub-surface layer, we can evaluate $\eta_h(0, t)$, based on the relation between $N(0, t)$ and $\eta_h(0, t)$ of equation (2), and can determine J from equation (16).

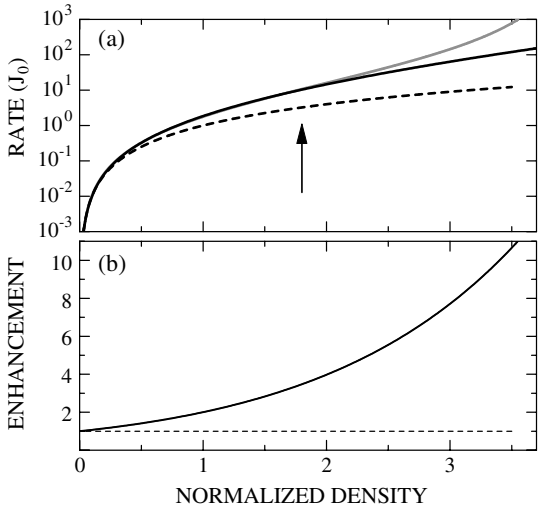

Figure 20. (a) The bond-rupture rate calculated as a function of normalized density n ($=N(0)/Z$) of valence holes in the sub-surface layer. The solid curve is the result of numerical calculation of equation (11), and the grey curve is the result of the approximated form for moderate density (equation (14)). The broken curve represents the square of n. (b) The ratio of the solid curve relative to the broken curve, showing the enhancement of the rate due to quantum statistics of valence holes (after [77]).

Since there are no analytical expressions of $F_{1/2}(\eta)$ in the general case, J cannot be expressed in a simple analytical form as a function of the hole density. However, for the case where $\eta_h(0)$ is smaller than two, we can use Ehrenberg's expression for $F_{1/2}(\eta_h)$:

$$F_{1/2}(\eta) = \frac{2\sqrt{\pi}\exp(\eta)}{4+\exp(\eta)}. \tag{18}$$

In this regime of excitation density, the relation between the hole density and the reduced quasi-Fermi level simplifies, and we can express J as

$$J(t) = J_0\left\{\frac{Z_h}{N(0,t)} - 0.25\right\}^{-2}. \tag{19}$$

In the case of Si, where $Z_h = 1.04 \times 10^{19}$ cm^{-3} at room temperature [85], the above conventional expression may be valid for hole densities up to $\sim 2 \times 10^{19}$ cm^{-3}.

In figure 20(a), we present the calculated results of equation (19), as a function of the normalized hole density n_h ($n_h = N(0,t)/Z_h$) in the sub-surface layer, and compare it with the results from the exact numerical solution of equation (16). It is clear that the approximate form for the rate of THL is valid for n_h less than 1.8, and is applicable to the experimental results studied so far. It is also clear that J deviates from the quadratic relation for a weak excitation condition around $n_h \sim 0.01$. The deviation, or the enhancement of J due to hole quantum statistics, is shown in figure 20(b) for comparison.

In the original formulation by Sumi, the rate of forming a two-hole localized state and the rate of bond rupture are the same. However, as shown in section 4.1, the yields of In- and P-bond rupture on InP(110)-(1 × 1) are different, although they are bonded with each other by the same bond. Then, it is more general to introduce a factor β that represents the relative efficiency of bond rupture of a particular species per two-hole localization event. Also, the rate

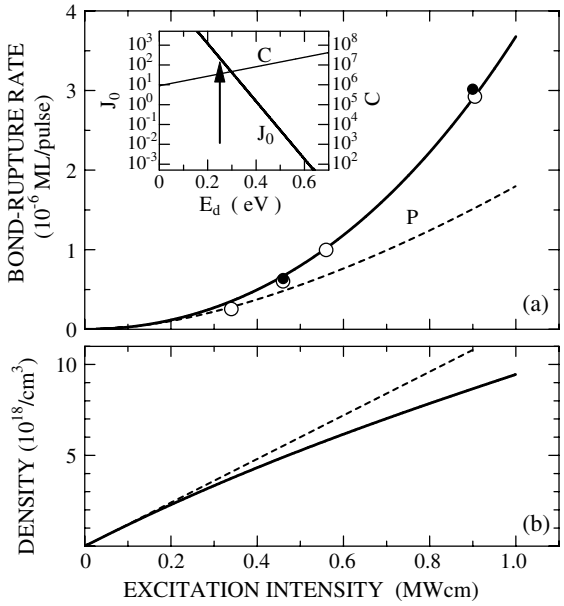

Figure 21. (a) The rate of bond rupture of P atoms on In(110)-(1 × 1) as a function of the excitation intensity, determined by STM observation of irradiated surfaces (●) and by desorption measurements (○) taken from [12]. The solid curve is the calculated results of equation (14), while the broken curve shows the simple quadratic dependence of the rate on the excitation density. The inset shows the relation between J_0 and E_d (after [77]). (b) The maximum density of valence holes in the sub-surface layer formed by a 5 ns laser pulse, calculated by solving equation (2) using $S = 1 \times 10^5$ cm s^{-1}. The other parameters used are given in the lists. The broken line shows the linear relation between $N(0)$ and the excitation intensity (after [77]).

of bond rupture is determined experimentally as the bond-rupture events per pulse. Therefore, we define here the per pulse bond-rupture rate K as

$$K = \beta \int_{-\infty}^{+\infty} J(t)\,\mathrm{d}t. \tag{20}$$

5.3. Comparison of the theory with experimental results

5.3.1. P-bond rupture on InP(110)-(1 × 1). As described in section 4.1, the electronic bond rupture of P and In atoms on InP(110)-(1 × 1) can be induced under bulk-valence excitation at room temperature. The rate of bond rupture is dependent super-linearly on the excitation intensity. These surfaces have no intrinsic bandgap states. Also, the surfaces had low surface-defect concentrations less than 0.001 ML prior to excitation (hereafter we refer to such surfaces, with low defect concentrations, as LDC surfaces). Defect-induced band bending is negligible in LDC surfaces [86]. Therefore, bulk valence excitation shows three-dimensional features, associated with strong concentration gradients and carrier flows. As a first test of the theory presented in section 5.2, we analyse the bond rupture processes of P atoms on InP(110)-(1 × 1) LDC surfaces.

The rate of P-bond rupture per pulse as a function of I_{ex} for InP LDC surfaces has been obtained by desorption studies in a relative scale (figure 17). Definite quantitative correlation between STM results and desorption results in figure 16 has made it possible to obtain the absolute magnitude of the bond-rupture rate. In figure 21(a), the rate of P-bond rupture per pulse thus quantified is re-plotted as a function of I_{ex}.

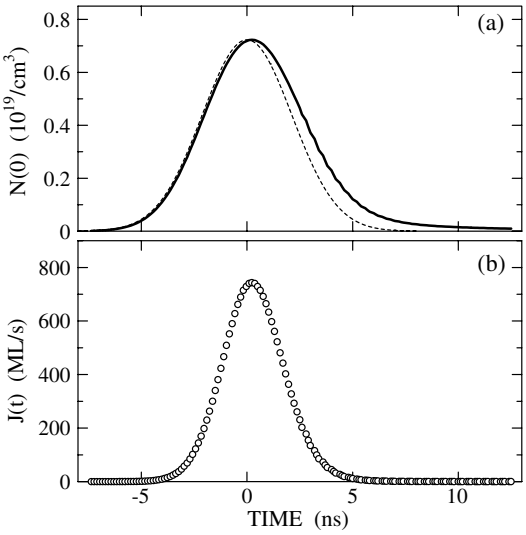

Figure 22. (a) Calculated valence hole density in the sub-surface layer $N(0)$ generated by a 5 ns laser pulse as a function of time. The broken curve shows the laser-pulse shape. (b) Calculated bond-rupture rate as a function of time (after [77]).

In theoretical calculation of J, we first solve numerically the particle balance equation for $N(0, t)$. Laser-induced heating was at most 30 K even for the highest excitation intensity used. Furthermore, because the heat diffusion length is much larger than the surface spatial range, we can neglect temperature gradient effects in equation (4). As shown by equation (6), D depends on the density through the Fermi-pressure factor A. However, A becomes only ∼20% larger than the low-density limit value of unity, for the density equal to Z_h, which corresponds to $\exp(\eta_h) \approx 2$. Since this effect is small in the present density range, we also neglect the density dependence of D. Similarly, we can also neglect the bandgap gradient dependence in the density regime smaller than Z_h. Therefore, the equation of particle balance can be reduced to a normal one-dimensional diffusion equation along the distance z from the surface. Then the generation term in equation (10) is given by

$$G(\vec{r}, t) = \frac{\Phi}{w(h\nu)}\alpha(1 - R)\exp\left(-\alpha z - \frac{4\ln 2}{w^2}t^2\right) \tag{21}$$

where w is the pulse width, α is the absorption coefficient, and R is the reflectivity. We use the standard boundary conditions [79, 82]:

$$N(z \to \infty, t) = N_h^0, \qquad \left(D\frac{\partial N}{\partial z}\right)_{z=0} = S_R N(0, t), \tag{22}$$

where N_h^0 is the concentration of holes under equilibrium conditions, and S_R is the surface recombination velocity. For the n-type specimens used in the experiment, the majority carrier (electron) concentration is 4.5×10^{15} cm^{-3} [12]. Therefore, N_h^0 is effectively set to zero. In the calculation of equation (7), S_R was treated as unknown, since its magnitude has not yet been determined for such LDC surfaces. To calculate $N(0, t)$ we use the absorption coefficient and reflectivity at 460 nm from [33], the radiative recombination rate (1.2×10^{-10} cm^3 s^{-1}) and the Auger recombination rate (9×10^{-31} cm^6 s^{-1}).[2]

In figure 22(a), we show the result of $N(0, t)$ thus determined as a function of time for $I_{ex} = 0.9$ MW cm^{-2}. Based on this result, we evaluated $\eta_h(0, t)$ as a function of time using

[2] These recombination parameters and effective density of states of valence band in InP were taken from the electronic archive of the Ioffe Physico-Technical Institute on 'New semiconductor materials: characteristics and properties', (http://www.ioffe.rssi.ru/SVA/NSM/).

$Z_h \approx 1\times10^{19}$ cm^{-3}. The maximum value of ψ_h ($=kT\eta_h(0)$) for the highest excitation intensity is +0.03 eV, which is considerably less than the calculated valueS of E_T (=0.13 eV) and U (=0.83 eV) for InP(110)-(1 × 1) [87]. Therefore, equation (16) can be applied for the present analysis. Also, since the maximum value of $N(0, t)$ is less than $2Z_h$ for the highest excitation intensity, we can use the approximated form of J of equation (19) to calculate the bond-rupture rate $J(t)$. The result of $J(t)$ for $I_{ex} = 0.9$ MW cm^{-2}, at constant J_0, is shown in figure 22(b). By integrating $J(t)$ with respect to time, we determine the bond-rupture rate $K(I_{ex})$ per pulse for a given intensity I_{ex}, based on the definition of equation (20). The calculated results of $K(I_{ex})$ are shown by the solid curve in figure 21(a). In the figure, it is clear that the calculated $K(I_{ex})$ is super-linear with respect to I_{ex}, and can reproduce the experimental results obtained for InP LDC surfaces.

To examine the super-linear nature of $K(I_{ex})$ further, we show the calculated maximum value of $N(0)$ as a function of I_{ex} in figure 21(b). The density tends to saturate at higher excitation intensities due to effective radiative recombination in this crystal. When we compare $K(I_{ex})$ with the square of n_h (the broken curve in the figure), it is evident that the bond-rupture rate depends more strongly on I_{ex} then the square of n_h, showing an quantum statistical effect of dense valence holes as expressed by the factor $\exp(2\eta_h)$.

In the evaluation of $K(I_{ex})$, we assumed $J_0 = 2.4 \times 10^2$ s^{-1} (with $y = 3/4$) as fit from the absolute magnitude of the STM results. Since the quantity J_0 ($=C\exp(-E_d/kT)$) in equation (16) is the factor to determine the absolute magnitude of the rate, quantitative examination of this constant provides an additional test of the theory. The magnitude of C for P-bond rupture on InP(110)-(1 × 1) can be calculated using equation (11) by inputting parameter values, most of which are obtainable from published data [87]. In the inset of figure 21(a), we plot the calculated value of J_0 as a function of E_d. The dependence is mainly determined by the exponential term of E_d, although the magnitude of C varies somewhat with E_d. For InP(110)-(1 × 1), the first hole is localized to form a metastable state on the highest occupied surface state (S_1) composed of s-like dangling bonds of anion atoms. The electronic structure of S_1 has been determined by photoelectron spectroscopy [88, 89]. The S_1 state is located 0.2 eV below the VBM at the $\bar{\Gamma}$ point of the surface Brillouin zone, and shows a dispersion width of about 0.8 eV. Therefore, we can take the average energy of 0.6 eV to be the level of the localized state. However, the energy of E_d is less than the average energy because the lattice relaxes upon hole localization. Although the lattice relaxation energy is not reported for hole (or electron) localization on semiconductor surfaces, one may expect an energy of about 0.2–0.3 eV [62]. Additionally, an enhanced ionicity of the surface bonds due to net charge transfer from In to P atoms in the (1 × 1) surface structure may lead to a larger lattice relaxation energy upon carrier localization from significant optical-phonon contributions [90]. The plot in the inset of figure 21(a) shows that E_d, corresponding to $J_0 = 2.4 \times 10^2$ s^{-1}, is about 0.25 eV, which suggests a lattice relaxation energy of 0.35 eV. As discussed above, this is a highly likely energy for hole localization on the surface. Therefore, the present theory reasonably describes not only the super-linear dependence of the bond-rupture rate on I_{ex}, but also its absolute magnitude.

In order to examine the validity of the present theory further, we analyse the bond-rupture rate as a function of surface-defect concentration. As shown in section 4.1, the rate of surface bond rupture depends on the concentration of surface vacancy sites. On n-type InP surfaces, P vacancies are charged negatively [69] such that they interact effectively with valence holes. Therefore, precise analysis of the effect of surface vacancies may provide a crucial test for the present theory. Although bond breaking at originally perfect sites, and at sites near pre-existing defects, takes place within an exciting laser pulse, the rate at perfect sites has been deduced unambiguously by introducing the total number density N, as in section 4.1. The

N thus determined has been shown in figure 13 as a function of number of incident laser pulses. From the plot, we can evaluate the rate of bond rupture from the slope of N. An initial slope of 3×10^{-6} ML/pulse is reduced to 2.3×10^{-7} ML/pulse at the surface excited up to 7000 laser shots, where the total surface-vacancy site density (V) increases up to 0.034 ML. Since the reduction in N_0 of equation (17) is negligible for $V = 0.034$ ML, it is clear that the factor $\exp(2\eta_h)$ decreases sharply with increasing defect concentration. In view of the effective interaction between valence holes and negatively charged surface vacancies, it is possible that hole localization around pre-existing P vacancies may serve to enhance bond breaking near defects. Such an effect would lead to efficient formation of vacancy clusters as described in section 4.2. On the other hand, defect-assisted hole localization reduces the density of valence holes in the sub-surface region. Because of a strong dependence of $\exp(2\eta_h)$ on $N(0)$, a small reduction of $N(0)$ could significantly decrease the magnitude of K. Therefore, the result in figure 13 is qualitatively consistent with the THL mechanism of bond rupture.

Quantitatively, hole trapping by pre-existing vacancies can be treated by introducing a vacancy-concentration dependent term of S_R; for damaged surfaces,

$$S_R(V) = S_0 + \gamma V. \tag{23}$$

The symbol γ represents the average trapping velocity per surface vacancy. Based on the experimentally determined total vacancy-site densities, we solved equation (7) with the $S_R(V)$ of equation (23) to have $N(0, t)$ on the surfaces with a given surface vacancy concentration. Then, K is evaluated, similar to the case of LDC surfaces. The result is shown by the solid curve in figure 13; it can describe reasonably the growth curve of N or the bond-rupture rate as a function of V. The magnitude of γ obtained by the fitting procedure is 3.7×10^{-8} cm^3 s^{-1}, which is larger, by more than a factor of 100, than the magnitude of $S_0/N_0(2 \times 10^{-10}$ cm^3 s$^{-1})$ for a perfect surface. The large value may reflect an effective interaction between valence holes and negatively charged pre-existing surface vacancies. Thus, the proposed theoretical model of THL can reproduce quantitatively the experimental results of excitation-induced bond breaking not only on InP(110)-(1 × 1) surfaces with low defect concentration, but also on the surfaces where interaction between valence holes and surface defects is significant.

5.3.2. Si-bond rupture on Si(111)-(2 × 1). The Si(111)-(2 × 1) surface is one more example where valence excitation induces the intrinsic surface bond rupture, as described in section 3.3. On this surface, the lowest valence excitation at 1.16 eV generates vacancies at Si_{up} sites with the rate dependent super-linearly on I_{ex}, as shown in figure 11. Silicon has an extremely small absorption coefficient ($\sim$11 cm^{-1}) at 1.16 eV such that optical excitation should be uniform and carrier diffusion from the surface to the bulk is negligible. However, fast surface recombination on this surface [77] can induce a density gradient in the valence hole density leading to net transport from the bulk to the surface. This process could enhance surface bond rupture. Analysis of experimental results on Si(111)-(2 × 1) can therefore provide another test of our theory that includes the effects of hole diffusion.

Before analysing the results, we briefly discuss the possible effects of band bending on this surface. The Fermi level of the n-type surface is pinned 0.38 ± 0.1 eV above the VBM [1] leading to upward bending and an accumulation of photogenerated holes in the surface region. This initial accumulation of surface valence holes may explain the enhanced bond-rupture rate observed for n-type surfaces [11]. However, as discussed already, the band becomes flattened due to photovoltaic effects under intense excitation [1]. Therefore, photogenerated carriers are subject to flat-band conditions and the theory in section 5.2 should apply.

To evaluate the role of bulk to surface hole diffusion, we solved the equation of particle balance numerically using similar boundary conditions as used for InP. We used reported

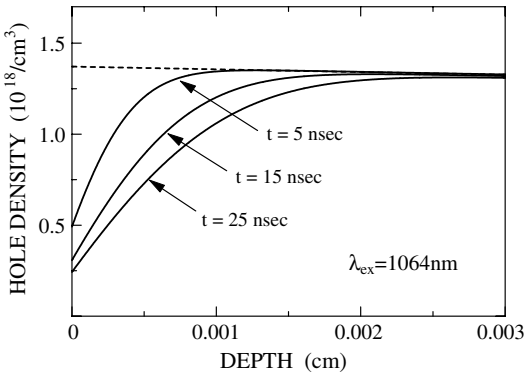

Figure 23. Calculated spatial distributions of the valence-hole density at respective times after 3.5 ns pulse excitation of a Si crystal (after [77]). The broken curve shows the concentration gradient governed by the absorption coefficient (without any effects of hole diffusion).

values for the absorption coefficient (11 cm^{-1}), reflectivity (0.30), ambipolar diffusion constant (18 $cm^2\ s^{-1}$), and Auger recombination coefficient (3×10^{-31} $cm^3\ s^{-1}$) [82], and treated the surface recombination velocity as an unknown parameter. In figure 23, we plot the spatial distribution of $N_h(z, t)$ at several time delays after 3.5 ns pulse excitation for the case of $S_R = 5 \times 10^4$ cm s^{-1}. Because of slow Si carrier decay rates, the density at the surface can reach $\sim 10^{18}$ cm^{-3} at the end of the highest intensity 3.5 ns pulses. The gradual decay of $N_h(0, t)$ results from slow decay rates and from persistent hole diffusion from the bulk to the surface, as seen in figure 23. Since the maximum density calculated is smaller than Z_h, equation (19) is applicable. We evaluated the bond-rupture rate K for a given excitation intensity by integrating $J(t)$ with respect to time. The calculated rates are plotted (solid curve) in figure 11. Again, the calculated results fit the experimental data reasonably well.

In order to fit the simulated results to the experimentally determined absolute value of K, we used the values $J_0 = 3.5 \times 10^4$ s^{-1} and $S_R = 5 \times 10^4$ cm s^{-1}. We did not try to obtain the best fit, since a rather wide range of S_R (from 5×10^3 to 8×10^4 cm s^{-1}) gave a similar non-linear dependence. On this surface, the surface π band localizes valence holes to form the first-hole localized state. The π band is in near degeneracy with the VBM, and we assume that $E_d = 0$. Even in this case, we can still use the formula of equation (9), since $\eta_h \leqslant -5$ for the present range of hole densities and $\exp(-\eta_h) \gg 1$. The value of C calculated using literature data is 5×10^4 s^{-1}, which is consistent with the parameter used in figure 12. The surface recombination velocity used in the calculation is typically 5×10^4 cm s^{-1}, much smaller than the value of 3×10^7 cm s^{-1} evaluated for an n-type surface at the low-injection limit [77]. Halas and Bokor have pointed out the important role of the time-dependent surface photovoltage shift that governs surface recombination in the sub-nanosecond temporal domain on this surface [77]. This photovoltage shift should be taken into account if more detailed analysis of short-time valence hole localization is required, as in the case of fs laser excitation. From this point of view, in terms of a one-parameter surface recombination velocity, our present calculation may be too simple to describe the dynamics fully. However, the temporal width of our laser pulse is 3.5 ns, and bond-breaking processes last for a few tens of nanoseconds. Therefore, we may take the value as an overall average of the surface recombination velocity over nanosecond duration for valence hole relaxation under flat-band conditions.

5.4. A unified model of THL on electronic bond rupture on semiconductor surfaces

As shown above, the THL mechanism extended to non-equilibrated three-dimensional valence hole systems can describe successfully and quantitatively the experimental results observed for InP(110)-(1 × 1), and Si(111)-(2 × 1). In modelling THL, we considered the effects of photogenerated bulk-valence holes, and consequently effects of excitation wavelength were included only through the bulk absorption coefficient to control the valence-hole density (see equation (21)). On the other hand, the bond-rupture rates on Si(111)-(7×7) and Si(001)-(2×1) show the resonant-type features with respect to the excitation wavelength, and crucial roles of surface-specific transitions have been suggested. Therefore, we need to include the effects of the direct channel of surface-optical transitions on surface charge re-distribution in the modelling.

First, we examine possible physical factors underlying the differences between the two groups of surfaces in the light of the THL mechanism. On Si(111)-(7 × 7), the bonds of adatoms, which are threefold coordinated, are ruptured upon excitation. In view of the THL mechanism, it is essential to localize the first hole on one of the surface states consisting of bonds related to adatoms, since their bonding properties may change significantly only under significant local charge re-distributions. The dangling bonds of adatoms form the metallic surface state (S_1/U_1) within the bulk bandgap of Si, with a significant energy separation from the VBM. The metallic nature of the band, together with a substantial charge de-localization among dangling bonds of adatoms and rest atoms, may make the formation of the localized-hole state less likely. Also, the energy separation from the VBM may prevent valence holes from second-hole localization because of the large energetic mismatch. Therefore, we presume that the S_1 state cannot serve as the surface state localizing holes to induce adatom-bond rupture. The next highest band (S_2), located 0.2 eV below the VBM, consists exclusively of filled dangling bonds of the rest atoms. Although localization of the hole on the lone-pair state of a rest atom may give some changes in the bonding properties of neighbouring adatoms, the changes, if any, may be reduced substantially by the significant charge delocalization among dangling bonds in a unit cell. Therefore, the first-hole localization on the S_2 state may not be efficient to induce bond rupture of adatoms. These considerations lead us to presume that the first hole should be localized on the S_3 state consisting of adatom back-bonds to induce charge re-distributions sufficient to induce bond rupture of adatoms. The S_3 state is located 1.0 ± 0.2 eV below the VBM, substantially deeper than the π band of Si(111)-(2 × 1) and the S_1 band of InP(110)-(1 × 1).

In the case of Si(001)-(2 × 1), the D_{up} state consisting of Si_{up} dangling bonds is located 0.15 eV below the VBM [1, 76]. The energy level from the VBM is shallower than the S_1 state of InP(110)-(1 × 1). Therefore, the D_{up} state could be the surface state localizing the first hole. However, because of the dimer configuration, the possible effects of charge re-distribution by the first localized hole may be shared by two σ-bonded Si atoms to reduce the instability of two-hole localization. Therefore, the localized hole configuration of the dimer may not result in favourable system energetics for two-hole localization. In fact, experimentally, no bond ruptures are detected under excitation with photon energies below 1.9 eV, that induces bulk-valence excitation. Therefore, we may conclude that bond rupture of one Si atom of the dimer needs hole injection to one of the back-bonds, which is located around 1.2 eV below the VBM. Thus it appears that hole injections into deep surface states are necessary to induce bond rupture on Si(111)-(7 × 7) and Si(001)-(2 × 1) surfaces.

In the THL mechanism, the density of the first-hole localized state is governed by the factor of $\exp\left(-\left(E_d - \Psi_h\right)/k_B T\right)$. For the surface states in the energy range of 0.3 eV below the VBM, like the π state of Si(111)-(2×1) and the S_1 state of InP(110)-(1×1), the first-localized-

hole populations are substantial ($>10^{-5}$) at relatively low density of valence excitation with $\eta_h < 0$. However, for the deep surface states with the energies of ~1 eV below the VBM, the hole population is not practical (less than 10^{-12}), even if the density is high enough with $\eta_h \approx 5$. Therefore, in view of the negligibly low population of the first-hole localized state, it is not possible to induce bond rupture of adatoms on Si(111)-(7 × 7) and of Si_{up} of the Si dimer on Si(001)-(2 × 1) by the THL mechanism of pure valence excitation. This is, on one hand, consistent with the experimental observation that bulk valence excitation cannot lead to the bond rupture on these surfaces, as clearly demonstrated in figure 7.

As described as the introductory remarks of this section, both surface optical transitions and bulk transitions can be active under excitation at a given photon energy. Because of small absorption coefficients, surface optical transitions may not give significant effects on the hole density of the bulk-valence band. However, they can give substantial effects on the hole-injection process into the surface states, in particular into deep surface states localizing the first hole. When we add this direct-channel term $(N_d)_{st}$ of the first-hole injection, then the density of bonds localizing the first hole N_d can be generalized as

$$N_d = N_0 \exp(-(E_d - E_F)/k_B T) + (N_d)_{st}. \tag{24}$$

Since a deep surface state is overlapped with the projected bulk density of states in general, the lifetime τ of optically injected holes in the surface states may be short in general. Therefore, for ns-pulse excitation, temporal change of the injected-hole density is primarily governed by the fast decay processes characterized by τ. Then, $(N_d)_{st}$ can be expressed as

$$(N_d)_{st} = N_0 \sigma(\lambda)\phi\tau \tag{25}$$

where $\sigma(\lambda)$ is the cross-section of the surface-specific optical transition at the excitation wavelength λ, and ϕ is the photon flux of a laser pulse, respectively. Although τ is short, the absolute value may depend on λ, governed by energetic and momentum overlap between the surface states and the projected bulk density of states. In the case of Si(111)-(7 × 7), the S_3 band is split off from the bulk state in the momentum space around the $\bar{K}$ point of the surface Brillouin zone [1]. Therefore, τ of surface holes injected around this symmetry point may be longer than those at other points where the S_3 band is overlapped in momentum and energetic spaces. When we assume $\tau \approx 10^{-14}$ s and $\sigma \approx 10^{-16}$ cm^{-2}, then $\sigma(\lambda)\phi\tau \approx 10^{-5}$ can be estimated for a 10 ns laser pulse with $\Phi = 10$ mJ cm^{-2}. This value is larger by more than a factor 10^7 than the term $\exp(-(E_d - \Psi_h)/k_B T)$ at $\eta_h = 5$ for deep surface states 1 eV below the VBM. Then, the second term of equation (24) can dominate over the first term under intense excitation at particular excitation-wavelength regions. Once the first localized holes are populated, the dense bulk-valence holes generated synergistically can effectively induce second-hole localization, since E_T of the second hole is typically on the order of 0.1 eV. In such a case, the rate of bond rupture is given by

$$J = N_0\{\sigma\phi(\lambda)\tau\}C \exp(\eta_h), \tag{26}$$

as a result of synergistic effects of bulk and surface optical transitions. The generalized rate of THL given by equation (26) includes explicitly the excitation-wavelength dependent factor of $\sigma(\lambda)$ for surface optical transitions.

In order to examine the applicability of equation (26), we analyse quantitatively the bond-rupture rate of Si adatoms on Si(111)-(7 × 7) shown in figure 5. The magnitude of η_h was evaluated by solving the particle balance equation as in other cases, with S_R being a parameter. Since the maximum value of the quasi-Fermi level Ψ_h determined by calculations is less than 0.05 eV, the condition $\Psi_h < E_T < U$ is still satisfied. Therefore, we can use equation (16), and hence equation (26). For $E_d = 0.8$ eV, considering the lattice relaxation energy of 0.3 eV, the value of C calculated using literature data is 1.0×10^7 s^{-1}. For the other

constants in equation (25), we tentatively assumed that $\tau \approx 10^{-13}$ s and $\sigma \approx 10^{-17}$ cm^{-2}. The value of σ assumed is smaller by a factor of 10 than that at the peak of the $\pi \rightarrow \pi*$ transition of Si(111)-(2 × 1) [54]. For a 20 ns laser pulse at fluence of 23 mJ cm^{-2} at 600 nm, $\phi = 3 \times 10^{25}$ cm^{-2} s^{-1}, leading to $\sigma\phi\tau \approx 10^{-5}$. The calculated rate per pulse for $S_R = 1 \times 10^5$ cm s^{-1} is shown by the solid curve as a function of I_{ex} in figure 4, which describes well not only the observed super-linear dependence of the rate on I_{ex}, but also the absolute magnitude of the rate (within a factor of 10). Therefore, equation (26) is applicable to evaluate quantitatively the bond-rupture rate on the surfaces with deep surface states that localize the first hole. The bond rupture rate of Si dimers on Si(001)-(2 × 1) was also analysed successfully by using equation (26). It is evident that the bond-rupture rate given by the unified model of equation (26) shows a resonant wavelength-dependent feature corresponding to surface-specific optical transitions.

As described in section 3.1, the bond rupture process on Si(111)-(7 × 7) is characterized by exclusive monovacancy formation, although sites nearest to pre-existing defects may provide weakened-bond configurations that are more effective for bond rupture. This feature shows a strong contrast to efficient vacancy-cluster formation on Si(111)-(2 × 1) and n-type InP(110)-(1 × 1), where valence excitation is entirely responsible for the bond rupture. In view of the unified model of the THL mechanism in equation (26), this experimentally observed feature becomes one of the direct consequences of the mechanism, since optical hole injections that trigger THL take place with a resonant feature in the wavelength domain, but with a complete random feature in the real-space domain. Since the surface optical transition concerned is characteristic of the intrinsic surface electronic states, distorted adatom back-bonds near pre-existing defects have substantially small contributions in the Bloch state of the two-dimensional electronic system. Also, the lifetime of injected holes is short enough to prevent them from effective transport. Therefore, the first-hole localization near pre-existing defects may be avoided, rather than enhanced. Then, essentially random formation of adatom vacancies results on this surface, instead of forming vacancy clusters as in the case of mobile valence-hole localization on InP(110)-(1 × 1) and on Si(111)-(2 × 1). Thus, by including a synergistic effect of bulk and surface optical transitions, the THL mechanism can be generalized to describe quantitatively and consistently all characteristic features of excitation-induced structural instability on covalent semiconductor surfaces.

6. Summary

We have reviewed experimental results on excitation-induced structural instability on covalent semiconductor surfaces obtained by scanning tunnelling spectroscopy studies to elucidate structural changes at the atomic level and by post-ionization spectroscopy studies to probe desorption processes with high sensitivity. By combining these results systematically, we have revealed the initial bonding properties of atoms to be desorbed, the electronic transition that triggers the desorption, and identified unambiguously excited species responsible for the electronic bond rupture. The instability is characterized by local bond rupture at intrinsic surface sites. In this electronic process we have found important common features, together with significantly different characteristics that depend on specific surface properties. Based on these experimental results, we have proposed a mechanistic model for the instability. We extended the THL model, originally formulated by Sumi, first to describe the role of non-equilibrium three-dimensional valence holes, and then to include synergistic effects between surface and bulk optical transitions. Through the quantitative and successful analysis of the main results of photoinduced structural instability on typical surfaces, we have demonstrated that the proposed model systematically describes all important characteristic features obtained

in experimental studies for covalent semiconductor surfaces. Future development based on first principles theoretical modelling of the local structures of intermediate configurations formed in the electronic process and on extensive experimental studies of short-time carrier dynamics should provide further insight into the surface-specific behaviour of semiconductors.

Acknowledgments

The authors are grateful to Professor H Sumi, Dr W P Hess, Dr K Ishikawa, and Mr E Inami for valuable comments and stimulating discussions. We acknowledge kind permission to reproduce several figures from our previous works published in the journals of Elsevier and the American Physical Society. This work was supported by a Grant-in-Aid for Scientific Research from the Ministry of Education, Science, Technology, Sports, and Culture of Japan.

References

[1] Mönch W 1995 *Semiconductor Surfaces and Interfaces* (Berlin: Springer)
[2] Long J P, Goldenberg S S and Kabler M N 1992 *Phys. Rev. Lett.* **68** 1014
[3] Ishikawa K, Kanasaki J, Tanimura K and Nakai Y 1996 *Solid State Commun.* **98** 913
[4] Xu J, Overbury S H and Wendelken J F 1996 *Phys. Rev.* B **53** R4245
[5] Chen X H, Polanyi J C and Rogers D 1997 *Surf. Sci.* **376** 77
[6] Kansaki J, Ishida T, Ishikawa K and Tanimura K 1998 *Phys. Rev. Lett.* **80** 4080
[7] Kanasaki J, Iwata K and Tanimura K 1999 *Phys. Rev. Lett.* **82** 644
[8] Han B Y, Nakayama K and Weaver J H 1999 *Phys. Rev.* B **60** 13845
[9] Kwak H *et al* 1999 *Phys. Rev. Lett.* **83** 3745
[10] Kanasaki J, Nakamura M, Ishikawa K and Tanimura K 2002 *Phys. Rev. Lett.* **89** 257601
[11] Inami E, Ishikawa K and Tanimura K 2003 *Surf. Sci. Lett.* **540** L587
[12] Goto T, Kotake S, Ishikawa K, Kanasaki J and Tanimura K 2004 *Phys. Rev. Lett.* **93** 117401
[13] Persson B N J and Avouris Ph 1997 *Surf. Sci.* **390** 45
[14] Von Allmen M and Blatter A 1995 *Laser-Beam Interaction with Materials; Physical Principles and Applications* (Berlin: Springer)
[15] Becker R S, Golovchenko J A, Higashi G S and Swartzentuber B S 1986 *Phys. Rev. Lett.* **57** 1020
[16] Stritzker B, Pospieszczyk A and Tagle J A 1981 *Phys. Rev. Lett.* **47** 356
[17] von der Linde D 1988 *Ultrashort Laser Pulses* (*Springer Topics in Applied Physics* vol 60) ed W Kaiser (Berlin: Springer) p 113
[18] Itoh N and Nakayama T 1982 *Phys. Lett.* A **92A** 471
[19] Namiki A, Cho S and Ichige K 1987 *Japan. J. Appl. Phys.* 1 **26** 39
[20] Hattori K, Okano A, Nakai Y and Itoh N 1992 *Phys. Rev.* B **45** 8424
[21] Tolk N H, Traum M M, Tully J C and Madey T E (ed) 1983 *Desorption Induced by Electronic Transitions I* (Berlin: Springer)
[22] Kelly R and Dreyfus R W 1988 *Nucl. Instrum. Methods Phys. Res.* B **32** 341
[23] Kanasaki J, Okano A, Ishikawa K, Nakai Y and Itoh N 1993 *Phys. Rev. Lett.* **70** 2495
[24] Dubreuil B and Gilbert T 1994 *J. Appl. Phys.* **76** 7545
[25] Kanasaki J, Mikasa N and Tanimura K 2001 *Phys. Rev.* B **64** 035414
[26] Takayanagi K, Tanishiro Y, Takahashi M and Takahashi S 1985 *Surf. Sci.* **164** 367
[27] Losio R, Altmann K N and Himpsel F J 2000 *Phys. Rev.* B **61** 10845
[28] Ishikawa K, Kanasaki J, Nakai Y and Itoh N 1996 *Surf. Sci. Lett.* **349** L153
[29] Poate J M and Mayer J W (ed) 1982 *Laser Annealing of Semiconductors* (New York: Academic)
[30] Wolkov R and Avouris Ph 1988 *Phys. Rev. Lett.* **60** 1049
[31] Uchino H, Huang D, Grey F and Aono M 1993 *Phys. Rev. Lett.* **70** 2040
[32] Kanasaki J and Tanimura K 2002 *Phys. Rev.* B **66** 125320
[33] Aspnes D E and Studna A A 1983 *Phys. Rev.* B **27** 985
[34] Aspnes D E and Studna A A 1972 *Solid State Commun.* **11** 1375
[35] Uhrberg R I G, Hansson G V, Nicholls J M, Persson P E S and Flodstrom S A 1985 *Phys. Rev.* B **31** 3805
[36] Martensson P, Ni W-X, Hansson G V, Nicholls J M and Reihl B 1987 *Phys. Rev.* B **36** 5974
[37] Nicholls J M and Reihl B 1987 *Phys. Rev.* B **36** 8071

[38] Hamers R J, Tromp R M and Demuth J E 1986 *Phys. Rev. Lett.* **56** 1972
[39] Qian G-X and Chadi D J 1987 *Phys. Rev.* B **35** 1288
[40] Misewich J A, Heinz T F and Newns D M 1992 *Phys. Rev. Lett.* **68** 3737
[41] Busch D G, Gao S, Pelak R A, Booth M F and Ho W 1995 *Phys. Rev. Lett.* **75** 673
[42] Sumi H 1984 *Phys. Rev.* B **29** 4616
[43] Daum W, Ibach H and Muller J E 1987 *Phys. Rev. Lett.* **59** 1593
[44] Stich I, Payne M C, King-Smits R D, Lin J-S and Clarke L J 1992 *Phys. Rev. Lett.* **68** 1351
[45] Stich I, Terakura K and Larson B E 1995 *Phys. Rev. Lett.* **74** 4491
[46] Zener C 1932 *Proc. R. Soc.* A **137** 696
[47] Zimmermann F M and Ho W 1994 *J. Chem. Phys.* **100** 7700
[48] Hasselbrink E 1996 *Laser Spectroscopy and Photochemistry on Metal Surfaces* (*Advances in Physical Chemistry Series*) ed H L Dai and W Ho (Singapore: World Scientific)
[49] Shkrebtii A I and Del Sole R 1993 *Phys. Rev. Lett.* **70** 2645
[50] Cricenti A, Purdie D and Reihl B 1995 *Surf. Sci.* **331–333** 1033
[51] Suzuki Y, Ishikawa K and Tanimura K 2003 unpublished
[52] Wierenga P E, Sparnaay M J and von Silfhout A 1980 *Surf. Sci.* **99** 59
[53] Dürr M, Biedermann A, Hu Z, Hofer U and Heinz T F 2002 *Science* **296** 1838
[54] Chiarotti G, Nannarone S, Pastore R and Chiaradia P 1971 *Phys. Rev.* B **4** 3398
[55] Selci S, Chiaradia P, Ciccacci F, Cricenti A, Sparvieri N and Chiarotti G 1985 *Phys. Rev.* B **31** 4096
[56] Del Sole R and Selloni A 1984 *Phys. Rev.* B **30** 883
[57] Ancilotto E, Andreoni W, Selloni A, Car R and Parrinello M 1990 *Phys. Rev. Lett.* **65** 3148
[58] Rohlfing M and Louie S G 1999 *Phys. Rev. Lett.* **83** 856
[59] Inamie E, Ishikawa K, Kanasaki J and Tanimura K 2003 *Surf. Sci.* **528** 115
[60] Inami E and Tanimura K 2006 *Phys. Rev.* B at press
[61] Pospieszczyk A, Abel Harith M and Stritzker B 1983 *J. Appl. Phys.* **54** 3176
[62] Sumi H 1991 *Surf. Sci.* **248** 382
[63] Pankratov O and Scheffler M 1995 *Phys. Rev. Lett.* **75** 701
[64] Tanimura K and Kanasaki J 1999 *Proc. SPIE* **3618** 26
[65] Ebert Ph *et al* 1995 *Phys. Rev.* B **51** 9696
[66] Semmler U *et al* 2001 *J. Chem. Phys.* **114** 445
[67] Berkovits V L, Ivantsov L F, Makarenko I V, Minashvili T A and Safariv V I 1987 *Solid State Commun.* **64** 767
[68] Selci S, Cricenti A, Felici A C, Goletti C and Chiarotti G 1991 *Phys. Rev.* B **44** 8327
[69] Ebert Ph, Urban K and Lagally M G 1994 *Phys. Rev. Lett.* **72** 840
[70] Kanasaki J, Gotoh T, Inaki E, Ishikawa K and Tanimura K 2006 *Phys. Rev.* B at press
[71] Qian M C *et al* 2003 *Phys. Rev.* B **67** 035308
[72] Tanaka S and Tanimura K 2003 *Surf. Sci.* **529** L251
[73] Ramaker D E, White C T and Murday J S 1982 *Phys. Lett.* A **89** 211
[74] Yasui A, Uozumi T and Kayanuma Y 2005 *Phys. Rev.* B **72** 205335
[75] Anderson P W 1975 *Phys. Rev. Lett.* **34** 953
[76] Weinelt M, Kutschera M, Schmidt R, Orth C, Fauster T and Rohlfing M 2005 *Appl. Phys.* A **80** 995
[77] Halas N J and Bokor J 1989 *Phys. Rev. Lett.* **62** 1679
[78] Long J P, Sadeghi H R, Rife J C and Kabler M N 1990 *Phys. Rev. Lett.* **64** 1158
[79] Tanimura K, Inami E, Kanasaki J and Hess W P 2006 *Phys. Rev.* B at press
[80] Sommerfeld A 1952 *Vorlesungen uber Theoretische Physik V: Thermodynamik und Statistik* ed F Bopp and J Meixner (Diederich: Wiesbaden)
[81] Preston J S and van Driel H M 1984 *Phys. Rev.* B **30** 1950
[82] van Driel H M 1987 *Phys. Rev.* B **35** 8166
[83] Elsaesser T, Shah J, Rota L and Lugli P 1991 *Phys. Rev. Lett.* **66** 1757
[84] Goldman J R and Prybyla J A 1994 *Phys. Rev. Lett.* **72** 1364
[85] Grove A S 1967 *Physics and Technology of Semiconductor Devices* (New York: Wiley)
[86] Ebert Ph, Urban K, Aballe L, Chen C H, Horn K, Schwartz G, Neugebauer J and Scheffler M 2000 *Phys. Rev. Lett.* **84** 5816
[87] Tanimura K 2004 *Phys. Rev.* B **69** 033301
[88] Sorba L, Hinkel V, Middelmann H U and Horn K 1987 *Phys. Rev.* B **36** 8075
[89] Qu H, Kanski J and Nilsson P O 1991 *Surf. Sci.* **255** 237
[90] Ueta M, Kanzaki H, Kobayashi K, Toyozawa Y and Hanamura E 1986 *Excitonic Processes in Solids* (*Springer Ser. Solid-State Sci.* vol 60) (Berlin: Springer) chapter 4